EFFECTS OF ELECTROMIGRATION ON THE RELIABILITY OF

RADIO FREQUENCY MICROELECTRO MECHANICAL SWITCHES

By

Naveen Kishore Karri

RECOMMENDED: Chuen-Lin Lin

Jonah Lee

Advisory Committee Chair

Chair, Department of Mechanical Engineering

APPROVED: John Aspnes

Dean, College of Engineering and Mines

Dean of the Graduate School

December 24, 2004

Date

EFFECTS OF ELECTROMIGRATION ON THE RELIABILITY OF RADIO FREQUENCY MICROELECTRO MECHANICAL SWITCHES

A

THESIS

Presented to the Faculty
of the University of Alaska Fairbanks

in Partial Fulfillment of the Requirements
for the Degree of

MASTER OF SCIENCE

By

Naveen Kishore Karri, B. Tech.

Fairbanks, Alaska

December 2004

Abstract

Radio Frequency (RF) Micro-Electro-Mechanical System (MEMS) switches have many advantages over semiconductor switches. Despite these advantages they are not implemented in reliability demanding space, defense and commercial applications because of reliability concerns. Although some failure modes have been identified so far, other failure modes are still under research. Electromigration, a well-known failure mechanism in interconnects, was recently recognized as a possible cause of failure in micro-switches. However, there have been no instances of electromigration studies in the literature. This thesis presents a preliminary study on the electromigration failure and its impact on the lifetime of MEMS switches.

A simulation program that emulates the electromigration process was developed. Parametric studies were performed to study the impact of impact certain parameters on electromigration process. The combined effects of Joule heating and electromigration were analyzed. Unlike passivated interconnects, the micro-switch is cantilevered and suspended in an inert medium without encapsulation. The electromigration lifetime estimation program developed in this thesis is applicable to all such free structures.

Joule heating has been demonstrated to be a key factor in the electromigration failure of micro-switches. Results showed that the electromigration process is very slow at the beginning. After a certain time, the resistance is found to increase exponentially, increasing the temperature of the strip drastically toward failure. The same trend is also observed in a gold micro-switch, but with much slower rate of electromigration degradation, indicating a longer lifetime.

Contents

List of Figures

List of Tables

ACKNOWLEDGEMENTS

The author would like to express his sincere appreciation and thanks to Dr. Cheng-fu Chen for his thoughtful guidance, invaluable assistance and continual support during the course of this thesis. Special thanks go to Dr. Chuen-sen Lin for his co-advising. Heartfelt thanks go to professor Jonah Lee for initially providing the author an opportunity to work for the UAF Center for Nanosensor Technology. Appreciation and thanks also go to professor Doug Goering, the Chair of the Department for being helpful throughout the author's M.S course work.

Sponsorship of this work by the Center for Nanosensor Technology at the University of Alaska Fairbanks is gratefully acknowledged. The help and support from the Arctic Region Supercomputer Center is highly appreciated.

The author is also indebted to his friends, family and room-mates for their moral support in the course of his education.

Chapter 1: Introduction

Electromigration is a mass transport phenomenon in current carrying metallic conductors due to the momentum transfer between conducting electrons and diffusing metal atoms. It is a process of mass transfer when the current density in metals reaches a threshold value, usually 5 $\times 10^5$ A/cm^2 for most materials [1]. Electromigration is found to be a major failure mode in thin film interconnects [2], [3]. Though electromigration has been widely studied in passivated thin film interconnects, very little literature has been published for studying electromigration failure in unpassivated micro structures like Radio Frequency Micro Electro Mechanical System (RF MEMS) switches.

RF MEMS switches are characterized by their high isolation, low insertion loss, large bandwidth and unparalleled signal linearity. They are relatively simple to control, very small in size and have very little power consumption. Despite these benefits, RF MEMS switches are not yet seen in commercial products because of reliability issues [4]. A few failure modes have been already identified and well understood, yet there still exist other unknown failure modes which may limit their deployment in many applications. These micro switches usually carry a few milli-amperes of current signals, which are equivalent to having a very high current density in the conductor. As the current density is higher than 1×10^5 A/cm^2, electromigration may pose a threat to reliability in these switches. Recently some researchers [5], [6] have mentioned such a possibility of electromigration damage in RF MEMS switches, but no further work has been done regarding this issue. Also it is unclear whether the electromigration may eventually lead to failure of microswitches.

Another important issue is, that the electromigration in microswitch beam structures differ [7] from that occurring in passivated thin film interconnects in two ways: (1) the micro beams are polycrystalline in structure and are not deposited on substrate; (2) as the beams are usually suspended in an inert medium (e.g., hermetic packages), the Joule heat

generated is not easily dissipated. Hence it raises the beam temperature, and consequently the electromigration process will be accelerated. As there are no instances of electromigration research under these situations, this thesis presents a preliminary work on the study of electromigration failure in RF MEMS switches.

The first part of the thesis deals with the RF MEMS switches in their basic design and mechanical reliability under deformation and shock. The second part, as the major contribution of the thesis, deals with the reliability of MEMS switches under electromigration. This section contains detailed formulations of electromigration life time analysis, the life time estimations at various temperatures, and current density levels and comparative study using Aluminum and Gold.

1.1 The Beginning of RF MEMS

The market for wireless personal communication devices has expanded so dramatically in the past two decades that the focus of research in the microwave and millimeter wave areas has shifted towards consumer applications, from the more traditional defense related products. Accordingly, the production volume has increased many times, while power handling capacity required for these systems has considerably decreased. These developments paved the way for increased application of microelectromechanical systems (MEMS) in many current *radio frequency* (RF), micrometer and millimeter wave systems. Such devices are termed as RF MEMS, although they encompass all miniaturized devices. The processing techniques for MEMS systems have improved significantly over the years. Apart from having the advantages of bulk production, and being miniaturized, these can often lead to more efficient systems compared with conventional ones [8].

The need for MEMS based systems for RF and microwave applications arises from the limitations of existing devices. Many MEMS based microwave components are aimed at

reducing *insertion loss* and increasing *bandwidth* and this aspect is most valid for RF MEMS switches. Conventional RF switching systems such as PIN diodes and transistors were found to be inefficient at higher frequencies. MEMS based RF switches with very low actuation voltage and virtually zero power consumption are the emerging devices, standing as a solution to aforementioned inefficiencies.

The term RF MEMS refers to the design and fabrication of MEMS for RF integrated circuits. It should not be interpreted as the traditional MEMS devices operating at RF frequencies. Microswitches are an important part of all RF MEMS devices. There are two distinct parts to an RF MEMS switch: the actuation (mechanical) section and the electrical section. The forces required for the actuation can be obtained using electrostatic, magnetostatic, piezoelectric or thermal designs. The movement for switches can be either vertical or horizontal depending on their layout. As for the electrical part, a MEMS switch can be placed in either series or shunt configurations and can be a metal-to-metal contact or a capacitive contact switch. This means one can build at least 32 (2×2×2×4) different types of MEMS switches using different actuation mechanisms, contact and circuit implementations [9]. Electrostatic actuation is the most prevalent technique in use today due to its virtually zero power consumption, small electrode size, thin layers used, relatively short switching time, and 50-200μN of achievable contact forces.

1.2 Classification of RF MEMS Switch

RF MEMS switches can be categorized based on the types of contact, their actuation methods, and their configurations. Two types of contact presented in RF MEMS switch designs are the metal-to-metal contacts and metal-insulator-metal contacts. The metal-to-metal contacts, also referred to as ohmic or direct contacts, can be found in cantilever-type MEMS switches. The signal in this microswitch is propagated when the two metal

contacts touch together such that electrical current passes through the established interface. Figure 1.1 illustrates the basic concept of a contact type RF MEMS switch.

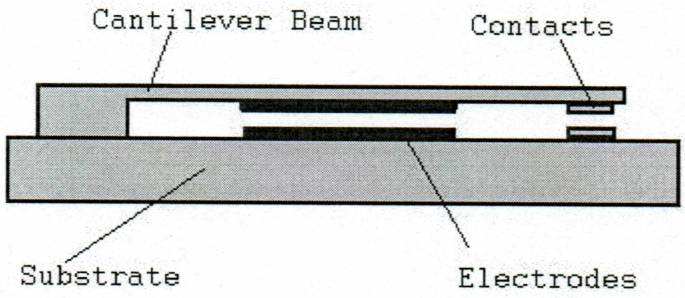

Figure 1.1: Schematic of a resistive type RF MEMS switch.

The metal-insulator-metal contact switches are sometimes referred to as capacitive microswitches or membrane switches. The capacitance built up between the electrode on a membrane and electrode on the substrate, via the applied voltage, is used as the means of actuating the micro-switch. This is illustrated in Figure 1.2. In this kind of switch a dielectric layer exists between two touching electrodes.

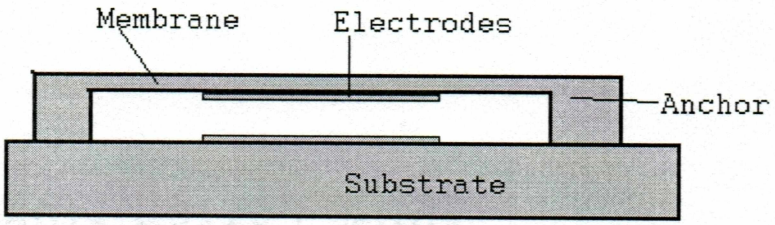

Figure 1.2: Schematic of a capacitive type RF MEMS switch

Classified by their actuation methods, MEMS switches can be electrostatically actuated, piezoelectric, thermally actuated or magnetically actuated.

- *Electrostatic:* Positive and/or negative charges, set by applied voltages between certain structural members, elicit Coulomb forces which produce motion.

- *Piezoelectric:* Applied voltages on structures induce fields to change their dimensions to communicate motion.

- *Thermal:* A current forced through an element causes it to heat up and expand, with the physical dimensional change being used to communicate motion.

- *Magnetic:* Magnet-induced or current- induced magnetic forces produce motion.

While a number of actuation mechanisms are under investigation for RF MEMS device applications, electrostatic actuation is the most mature, perhaps due to its use of surface micromachining, which is the most common technology utilized to produce electrostatic based actuators, and compatible with integrated circuit fabrication processes.

In terms of configurations, there are two basic switches used in RF to millimeter-wave circuit designs: the series or resistive switch and the shunt or capacitive switch.

The ideal series switch results in an open circuit in the transmission line when no bias voltage is applied (up-state position), and it results in a short circuit in the t-line when a bias voltage is applied (down-state position). Ideal series switches have infinite isolation in the up-state-position and have zero insertion loss in the down-state position. MEMS series switches are used extensively for 0.1 to 40 GHz (RF signal frequency) applications.

Figure 1.3 illustrates an inline DC-contact MEMS series switch with one contact area, along with its equivalent circuit configuration.

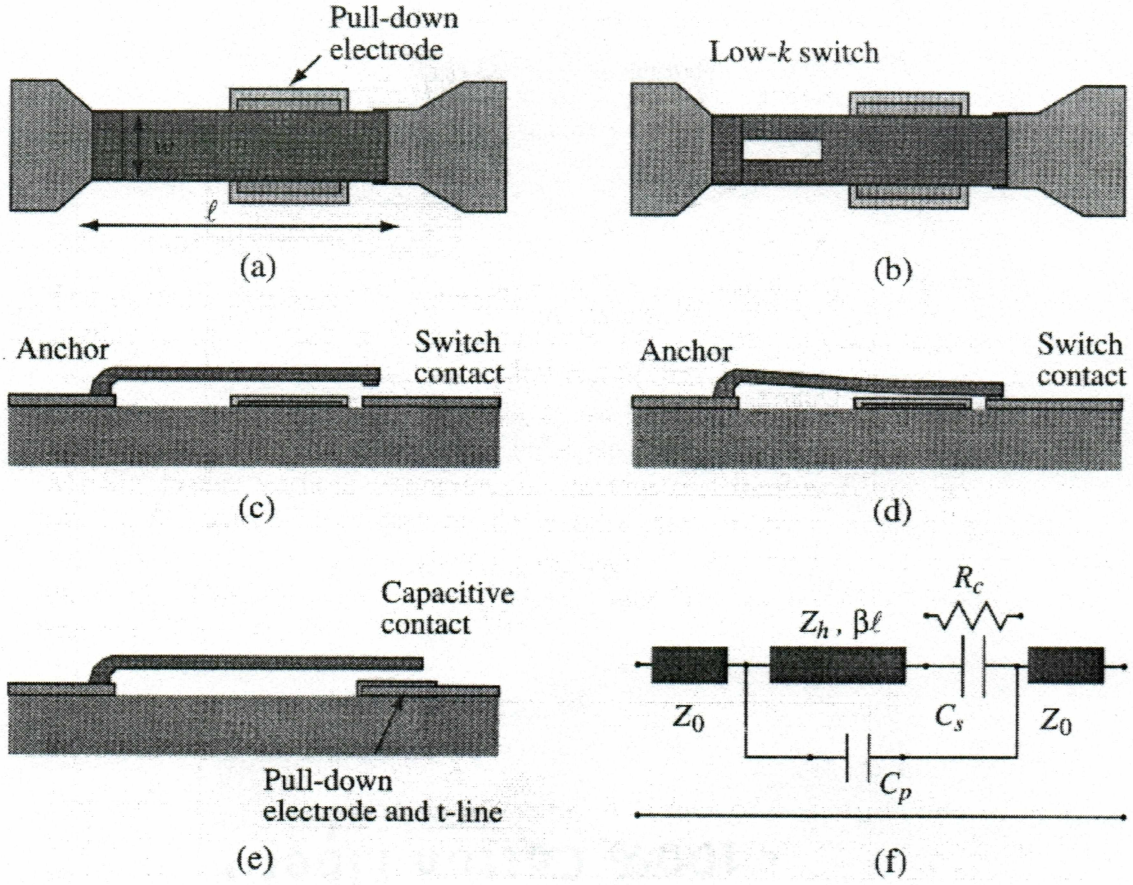

Figure 1.3 Inline DC-contact MEMS series switch with one contact area (a, b), cross-section in the up and down-state positions (c, d), cross section of a capacitive inline switch, generic circuit model (e, f) (Courtesy: Rebeiz & Muldavin [9])

The second type of configuration is shunt type. The shunt switch is placed in shunt between the t-line (transmission line) and ground. Depending on the applied voltage, it either leaves the t-line undisturbed or connects it to the ground. Therefore, the ideal shunt switch results in zero insertion loss when no bias is applied (up-state position) and infinite isolation when bias is applied (down-state position). Shunt capacitive switches are more suitable for higher frequencies (5-100GHz). Figure 1.4 illustrates a shunt type capacitive micro switch along with its equivalent circuit model

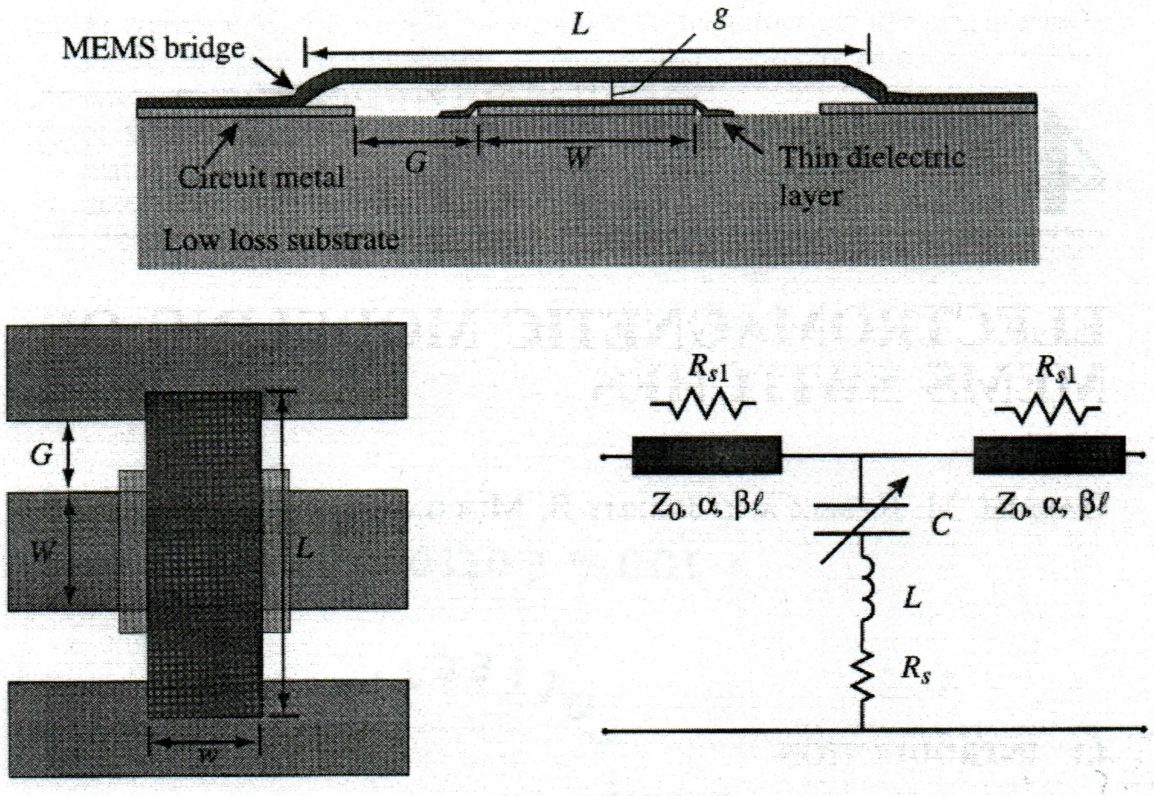

Figure 1.4: Shunt capacitive switch with equivalent circuit (Courtesy: Rebeiz & Muldavin [9])

1.3 Advantages of MEMS Switches

Traditional electromechanical switches, such as waveguide and coaxial switches, show low insertion loss, high isolation, and good power handling capabilities but consume high power and are slow and unreliable for long-life applications. Current solid-state RF technologies (PIN diode and FET based) are utilized for their high switching speeds, commercial availability, low cost, and ruggedness. Their inherited technology maturity ensures a broad base of expertise across the industry, spanning device design, fabrication, packaging, applications/system insertion and, consequently, high reliability and well-characterized performance assurance. Some parameters, such as isolation, insertion loss, and power handling, can be adjusted via device design to suit many application needs, but

at a performance cost. Insertion loss is the measurement of signal loss due to insertion of switch or any device in the circuit. Isolation refers to the amount that an unwanted signal is attenuated before it is detected at the port of interest. Higher isolation is desired as it eliminates the unwanted interference. For example, some commercially available RF switches can support high power handling, but require large, massive packages and high power consumption [10].

In spite of this design flexibility, two major areas of concern with solid-state switches persist: breakdown of linearity and frequency bandwidth upper limits. When operating at high RF power, nonlinear switch behavior leads to spectral regrowth, which smears the energy outside of its allocated frequency band and causes adjacent channel power violations (jamming) as well as signal to noise problems. The other strong driving mechanism for pursuing new RF technologies is the fundamental degradation of insertion loss and isolation at signal frequencies above 1-2 GHz.

The development of MEMS (Microelectromechanical Systems) technology makes it possible to fabricate electromechanical and microelectronics component in a single device. By utilizing electromechanical architecture on a miniature (or micro scale), MEMS RF switches combine the advantages of traditional electromechanical switches (low insertion loss, high isolation, extremely high linearity) with those of solid-state switches (low power consumption, low mass, long lifetime).

Table 1.1: Performance comparison of FETs, PIN diode and RF MEMS electrostatic switches [2]

PARAMETER	RF MEMS	PIN-DIODE	FET
Voltage(V)	20 – 80	± 3 – 5	3 – 5
Current (mA)	0	3 – 20	0
Power consumption (mW)	0.05 – 1	5 – 100	0.05 – 0.1
Switching time	1 – 300 μs	1 – 100 ns	1 – 100 ns
C_{up} (series) (fF)	1 – 6	40 – 80	70 – 140
R_s (series) (W)	0.5 – 2	2 – 4	4 – 6
Capacitance Ratio (C_{up}/C_{down})	40 – 500	10	n/a
Cutoff freq. (THz)	20 – 80	1 – 4	0.5 – 2
Isolation (1 – 10 GHz)	Very high	High	Medium
Isolation (10 – 40 GHz)	Very high	Medium	Low
Isolation (60 – 10 GHz)	High	Medium	None
Loss (1 – 100 GHz) (dB)	0.05 – 0.2	0.3 – 1.2	0.4 – 2.5
Power handling (W)	<1	<10	<10
3rd order intercept pt (dBm)	+66 – 80	+27 – 45	+27 - 45

Table 1.1 provides a comparison of MEMS, PIN-diode and FET switch parameters. Although a comparison between electrostatic MEMS switches and GaAs PIN diode and transistor switches is shown in the Table, it is hard to make an accurate comparison over a wide range of RF power levels, since the size of a diode or transistor can be easily increased for high power applications.

From Table 1.1, we can conclude that, though many of the electromechanical switches exhibit excellent RF characteristics such as low insertion losses and high isolation, typically up to several hundreds of megahertz, they have a very slow switching speed. Thus, electromechanical switches perform poorly when used as high-speed switches. For applications where the operational speed is more important than the power handling, solid state switches are preferred. The key reason for this slow switching speed is that the switching is performed by physically blocking or opening the transmission path in a

device. Other key disadvantages and research issues of MEMS switches include high actuation voltages and low RF power handling.

1.4 Application Areas of RF MEMS Switches

The leading characteristics of RF MEMS switches, i.e., the outstanding isolation and insertion loss at microwave frequencies, will make them a replacement to current GaAs switches in cellular telephones, resulting in much lower DC power consumption and longer battery life. They can also be used in phase shifters, which are essential for modern telecommunication, automotive, and defense applications, in low-loss tunable circuits (matching networks, filters etc), and in high performance instrumentation systems.

Telecommunication is the most sought application area for RF MEMS switches because it covers a broad range of frequencies, from below HF through VHF. The main uses of RF switches in the telecommunication industry are for signal routing, in impedance matching networks and for changing the gain of amplifiers. The specific applications at various wave bands include AM band (at the low end of MHz), commercial FM band (88-108 MHz), military handheld radio transceivers and cellular radios (900MHz and 2.4 GHz) and Bluetooth^{TM} (2.45 GHz) and other applications at frequencies ranging from KU-band (12.4-18GHz) to upper side of W band (75-110GHz) also require high quality RF switches. The RF components which incorporate the RF MEMS switches in telecommunications can be grouped as transmitters, receivers, antennas, and other transmission lines.

Though it is evident that RF MEMS switches can be readily used in defense or high-value commercial applications (satellite systems, base stations, etc.), their use in low-cost commercial systems is still under investigation due to their high fabrication cost, resulting from the hermetic packaging requirements and other reliability considerations.

The other aspect that is preventing their application in many commercial products is that they cannot be mass produced with existing technology and micro fabrication techniques.

1.5 RF MEMS Switch Current State of Technology

We have seen that RF MEMS can exhibit excellent performance at microwave frequencies, but suffer from reliability problems and the potential of relatively high-cost hermetic packaging. Now considering the pros and cons of MEMS switches from current state of technology, we have the following advantages [11], [12]:

- *Near-Zero Power Consumption:* Electrostatic actuation requires 30-80 V but doesn't consume any current, leading to very low power dissipation. But thermal and magnetic actuation switches consume a lot of current.
- *Very High Isolation:* RF MEMS switches fabricated with air gaps have very low off-state capacitance (2-4 fF). Also capacitive switches with capacitance ratio of 60-160 provide excellent isolation from 8 -100 GHz in frequency.
- *Very Low Insertion Loss:* RF MEMS metal-to-metal and capacitive switches have an insertion loss of 0.1 dB up to 100 GHz.
- *Linearity and Intermodulation products:* MEMS switches are extremely linear devices and thus result in very low intermodulation products in switching and tuning operations. Their performance is 30-50 dB better than PIN or FET switches.

Apart from advantages they also share the following disadvantages

- *Relatively low switching speeds:* The switching speeds of most electrostatic MEMS switches are 2-40μs and those of thermal/magnetic actuation switches are 200-3000μs, which is very low compared to those of semiconductor switches.
- *High voltage or high current requirements:* The electrostatic actuation MEMS switches require 30-80V for operation though they consume very low current. On

the other hand thermal/magnetic actuation switches require high currents 10-300mA though they can be activated with 2-5V.

- *Power handling:* Most MEMS switches cannot handle more than 200mW of power, although some switches have shown up to 500mW power handling capacity (Raytheon and Teravicta switches [13]).
- *Packaging:* MEMS switches need to be packaged in inert atmospheres (Nitrogen, Argon, etc.), and in very low humidity, resulting in hermetic and non hermetic seals. Hermetic packaging costs are currently relatively high, and the packaging technique itself may adversely affect the reliability of the MEMS switch.
- *Cost*: While MEMS switches have the potential of very low cost manufacturing, one must add the cost of the packaging and the high-voltage drive chip. Therefore it is hard to beat the cost of semiconductor switches, which is only a few cents at present.
- *Reliability:* The reliability of MEMS switches is 0.1-40 billion cycles. However, many systems require switches with 20-200 billion cycles. Also, the long term reliability (years) has not yet been addressed. It is now well known that the capacitive switches are limited by the dielectric charging that occurs in the actuation electrode, while the metal contact switches are limited by the interface problems between the contact metals, which could be severe under low contact forces. In electrostatic designs, the contact forces are around 40-100 μN per contact. It is important to note that the reliability and packaging issues have been the limiting factors to the quick deployment of RF MEMS switches, and they are currently under intense investigation. DARPA has initiated two programs in 2002 and 2003 to address these problems.

1.6 Thesis Motivation, Objectives and Contents

Although designers are approaching the optimal MEMS switch design, some failure modes still limit the design possibilities and adversely affect reliability of the micro

switches. The failure modes that have been identified and studied so far include creep, stiction, self pull-in, and wear [4]. In fact, many solutions were also proposed for the above mentioned failure modes. Though there are some disadvantages of RF MEMS switches when compared with semiconductor switches, as discussed in sections 1.4 and 1.6, they are not the key factors limiting their usage in many applications. Nevertheless the failure modes, and hence reliability, is the main factor limiting the deployment of MEMS switches into aerospace, defense, satellite communication and other high cost applications that demand very high reliability.

This thesis discusses a novel failure mode in micro switches called electromigration. In this thesis an attempt is made to study the electromigration failure of RF MEMS switches and their reliability. A simulation program was developed in order to study the effects of electromigration on the reliability of micro switches. A parametric study was also performed in order to understand the effects of various parameters that govern the electromigration process. The effects of electromigration on the switch lifetime, with and without Joule heating, were investigated.

Chapter 2 deals with the reliability of MEMS switches under deformation and shock. Some mechanical design aspects of switches were also presented in this chapter. In Chapter 3 the effects of electromigration on the lifetime of MEMS switches in the absence of Joule heating was studied. In this chapter the governing equations for electromigration were reviewed and a simulation program was developed for studying the influence of electromigration. A parametric study is also carried out for understanding the influence of various parameters on electromigration in micro switches. Chapter 4 includes the Joule heating effects on the electromigration reliability of RF MEMS switches. In Chapter 5 the results are summarized along with some conclusions. A few suggestions for future work are also included.

Chapter 2: Mechanical Reliability and Modeling of a RF MEMS Switch

This chapter deals with (1) the reliability of RF MEMS switches under mechanical forces and (2) the modeling of the micro-switch considered. The reliability of MEMS switches is of major concern for long-term applications and is currently under intensive study. Though the mechanical failure modes were thought to be dominant during the development of these switches (1990-1995), recent studies (2000-2003) have shown that these switches would be safe (perform without failure) under the major mechanical force environments like deformation, vibration and shock [14], [16]. In this chapter some analytical formulations and simulations were carried out to understand the reasons behind the operation of microswitches without failure. The simulation results provided good understanding of the reliability of MEMS switches under mechanical loads.

Apart from these mechanical failure modes, the other common failure modes observed in RF MEMS switches are found to be related to the metal contact used [17] in the DC-contact switches; as for capacitive switches, the reliability is limited by dielectric charging problems [18]. These failures were not studied in this thesis, as numerous solutions already were proposed by many authors regarding the stiction and dielectric charging problems [18-20].

2.1 A RF MEMS Switch Model

In this thesis, an inline DC-contact resistive type MEMS switch with one contact area, similar to one manufactured by Cronos Integrated Microsystems [21] (now MEMSCAP), was considered for analysis. Figure 2.1 shows a simplified cross-sectional view of the RF MEMS switch, which consists of a current-carrying cantilever beam anchored to a silica substrate.

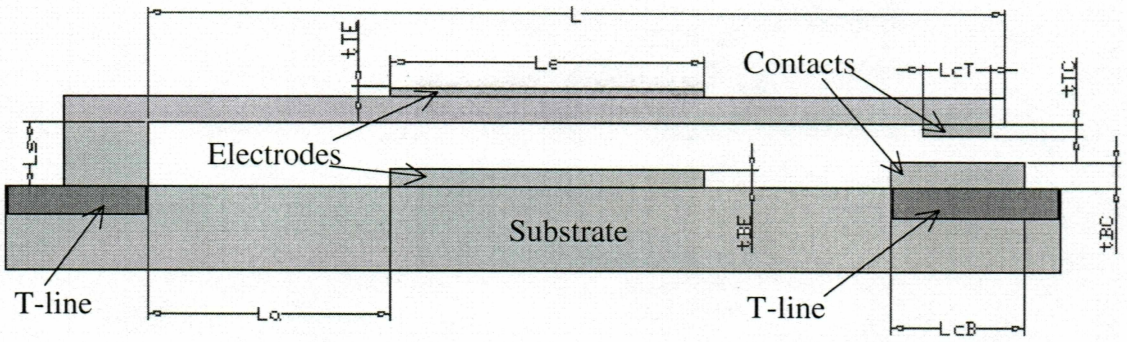

Figure 2.1: Schematic of a RF Switch, with dimensions labeled for Table 2.1 .

Table 2.1 lays out the dimensions of the switch for all the calculations in this chapter.

Table 2.1 Dimensions of the switch considered.

PARAMETER	DIMENSION
Beam Length, L	200.0 μm
Beam Width, w	20.0 μm
Beam Thickness	0.5 μm
Electrode Length, Le	50.0 μm
Beam Suspension gap, Ls	3.5 μm
Electrode distance from anchor, La	75.0 μm
Top Electrode Thickness, tTE	0.2 μm
Bottom Electrode Thickness, tBE	1.0 μm
Contact Gap, d	2.0 μm
Top Contact thickness, tTC	1.0 μm
Bottom Contact Thickness, tBC	0.5 μm
Top Contact Length, LcT	6.0 μm
Bottom Contact Length, LcB	12.0 μm

Aluminum (Al) and Gold (Au) are the materials considered for the model, with their material properties listed in Table 2.2. The contacts and the electrodes were also considered to be made of the same material. Here the cantilever beam carries the RF

signal current as it is in-line with transmission line. The electrostatic force between the electrodes causes the beam to deflect downward, bringing the contacts together to short the circuit.

Table 2.2: Properties of aluminum and gold [22].

Property	Aluminum	Gold
Young's Modulus (GPa)	70.0	83.0
Yield Strength (MPa)	310.0	205.0
Poisson's Ratio	0.35	0.44
Density (gm/cm^3)	2.70	19.30
Shear Modulus (GPa)	26.0	27.0
Thermal Conductivity (W/cm-K)	2.35	3.20
Thermal Expansion Coeff. (ppm/K)	23.10	14.20

2.2 Switch Design

Any electrostatic switch can be represented by an equivalent mechanical model shown in Figure 2.2, where g is the gap between the electrodes, K is the spring constant of the beam, and V is the actuating voltage.

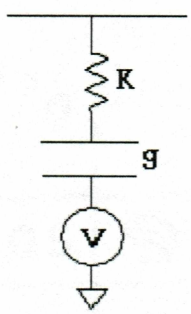

Figure 2.2: Equivalent mechanical model

The pull-down voltage (or the activation voltage) is given by [23],

$$V_p = \left(\frac{8Kg^3}{27\varepsilon_0 A} \right)^{\frac{1}{2}} \tag{1}$$

where K is the spring constant of the beam, g is the contact gap, ε_0 is the permittivity in the free space, and A is the area of the electrodes.

The spring constant of the beam can be found from the deformation of the beam under the applied electrostatic force. Though this electrostatic force acts as a uniformly distributed force on the electrodes, we can replace it by an equivalent point load acting at the geometric center of the top electrode. Figure 2.3 shows the deformation of the beam under the applied electrostatic force F.

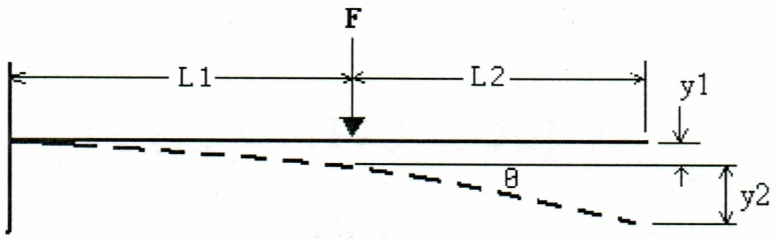

Figure 2.3: Deformation of the beam under electrostatic force 'F' .

Here the actual deformation at the contact includes two parts. The first part is the deformation of the length L1 from the anchor to the point of application of force. This is y1. The second part is the deformation of length L2 which remains straight. This deformation y2 can be obtained by finding the slope at L1.

y1 is given by solving the well known deflection equation,

$$EI \frac{d^2 \mathrm{y1}}{dx^2} = M \tag{2}$$

where E is Young's modulus of the beam material, I is moment of inertia of the beam cross section about its centroid and M is the bending moment.

Equation 2 can be solved by using the following two boundary conditions

(1) at x = 0, slope $\frac{dy1}{dx} = 0$

(2) at x = 0, y1 = 0

Hence the deflection at L1 is found to be

$$y1 = \frac{-FL1^3}{3EI} \tag{3}$$

The slope at L2 is,

$$\theta = \frac{-FL1^2}{2EI} \tag{4}$$

Therefore the deflection, y2 is:

$$\theta \times L2 = \frac{-FL1^2 L2}{2EI} \tag{5}$$

The deflection at the tip of cantilever beam is the sum of two above deflections y1 and y2

In our case the geometric center of the electrode coincides with the middle point of the cantilever beam, so L1 is equal to L2. The contact gap is 2 μm.

Therefore y1+y2 = -2 μm. (The negative sign indicates downward deflection.)

Let L1 = L2 = L μm

$$\text{Therefore, } y1 + y2 = \frac{-FL^3}{3EI} + \frac{-FL^3}{2EI} = \frac{-5FL^3}{6EI} = 2\times10^{-6} \text{ m} \tag{6}$$

The switch beam here is made of aluminum, E = 70 GPa and $I = \frac{bh^3}{12}$ where b is beam width (20 μm) and h is beam thickness (0.5 μm). The length Ll is half the beam length, 200 μm.

On substituting the values of I and L in Equation (6), the force required to have a deformation of 2 μm at the contacts is 14.0 μN. If the same beam is made of Gold with Young's modulus E = 83 GPa, the force required for actuation is 16.6 μN.

The spring constant is found as the ratio of the applied force to the deformation at the point of application and is k = F/y1.

By substituting y1 from Equation (3), the spring constants for Aluminum and Gold beams are:

$$k_{Al} = 14\ \mu N/0.8\ \mu m = 17.5\ N/m$$

$$k_{Au} = 16.6\mu N/0.8\ \mu m = 20.75\ N/m$$

These values are found to be in the general range of spring constants for RF MEMS switch beams [21]. Substituting these values of spring constants in Equation (1) results in pull-down voltages of 61 V and 67 V for Aluminum and Gold beams, respectively. These pull-down voltages are also in good agreement with the voltage range for MEMS switches in the literature [23].

2.3 Switch Reliability under Deformation

To analyze the reliability of the switch under electrostatic forces, the switch is simulated for stress and strain levels when subjected to cyclic loading. The cantilever beam is subjected to an alternating stress cycle when turned ON and OFF. Figure 2.5 illustrates the switch modeled in ABAQUS.

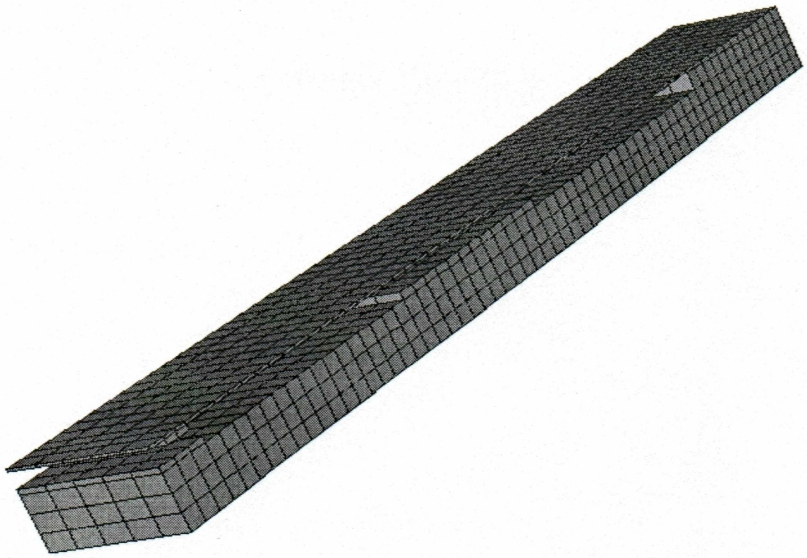

Figure 2.4: Switch finite element model in ABAQUS

Here the Al beam is considered and a concentrated force, which is equivalent to the electrostatic force on electrodes, is applied at the geometric center of the electrode. The simulation is carried out for two cycles with each cycle consisting of ON (force applied) and OFF (force released) states. In general simulation for two cycles would be enough to predict the life of any component subjected to cyclic loading under low cycle fatigue conditions, because, in low cycle fatigue, the lifetimes could be estimated from the incremental plastic strain between the first two cycles. Figure 2.5 illustrates the cyclic loading path applied in the simulation. Here the increment in accumulated plastic strain is noted from the first to the second cycle. This incremental plastic strain can then be used to predict the lifetimes under cyclic loading using the life predicting equations like the Coffin-Manson equation.

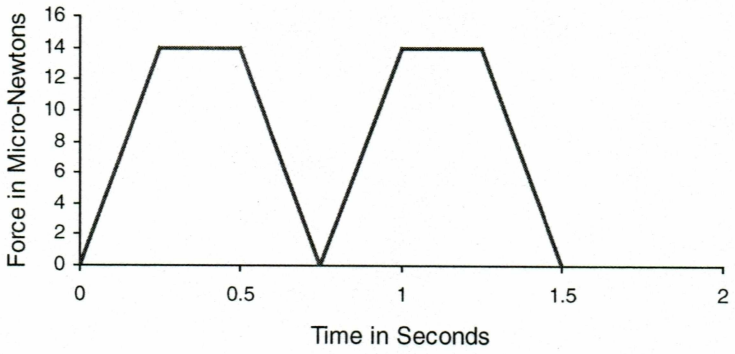

Figure 2.5: Load cycle considered in the simulation.

In order to get the equivalent plastic strains from ABAQUS we have to input the plastic region data into ABAQUS before the simulation. Table 2.3 shows true stress vs. true plastic stain data used in the simulations.

Table 2.3 True stress Vs. true plastic strain data for Al in the plastic region [24].

True Stress (MPa)	True Plastic Strain
310	0.0
350	0.0042
365	0.005
384	0.0166
400	0.025
425	0.333
450	0.05
490	0.075
518	0.1
550	0.15
560	0.156
570	0.157

Figure 2.6 shows the maximum stress levels in the switch during deformation. The maximum stress produced was found to be at the beam anchor and its value is 0.02 MPa

in each cycle. It is evident that the stresses produced during switch deformation were almost negligible compared to the yield strength of the aluminum (350 MPa), indicating that the beam is safe under the applied electrostatic forces. This is mainly due to the fact that the cantilever beam is only deflected by 2-3 μm which is relatively very small compared to the length of the beam.

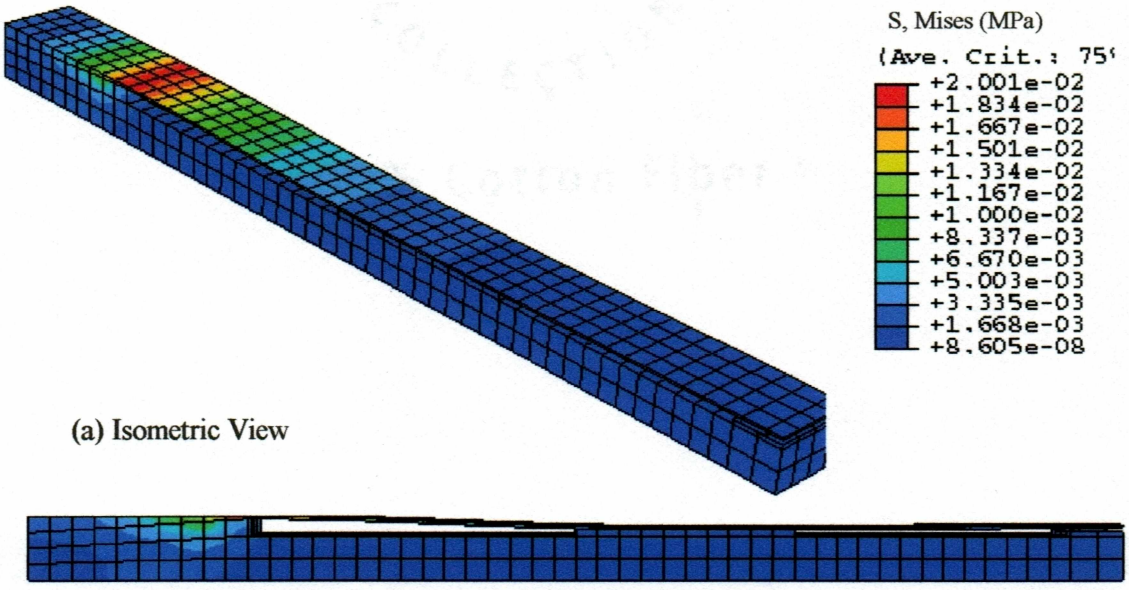

(a) Isometric View

(b) Deformed State Front View

Figure 2.6: Stress distribution in the micro switch at a deformed state.

Figure 2.7 shows the plastic strain increment in the two cycles. The plastic strains produced are zero in both cycles, as the stresses never reached plastic state in any of the cycles. Therefore the switch will operate within the elastic region and it can be concluded that the switch will operate for infinite cycles unless it fails under other dominant modes in between. These results also agree with the recent experimental results on MEMS reliability, in that most of the MEMS switches were already found to operate for billions of cycles with out failure [25-27].

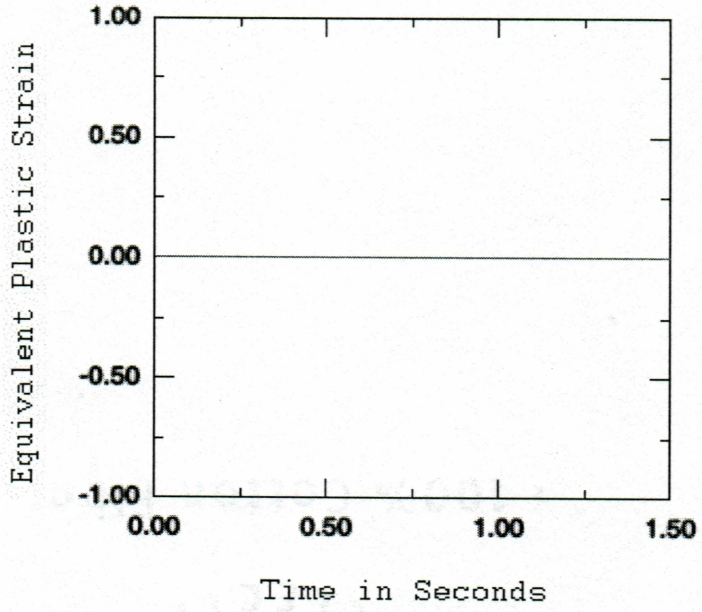

Figure 2.7: Accumulated plastic strain over two cycles

2.4 Reliability under Shock

To test the reliability of the switch under shock, a drop test was simulated and the stress distribution was observed for life time estimation with the Al beam. Here the switch is dropped from a height of 1 m. The beam is considered to be anchored to a silica substrate as described earlier. Figures 2.8 and 2.9 illustrate the peak stresses in the package and switch, respectively, during the drop test. It is clear from the figure that the maximum stress is reached in the beam is around 16.0 MPa and the maximum stress in the package (or substrate) is 36.5 MPa. Since the peak stress in the beam is far smaller than the yield stress (310.0 MPa), the switch is considered to be safe under a single mechanical shock. This result also agrees with the previous work on reliability of MEMS under shock and vibration environments [14-17].

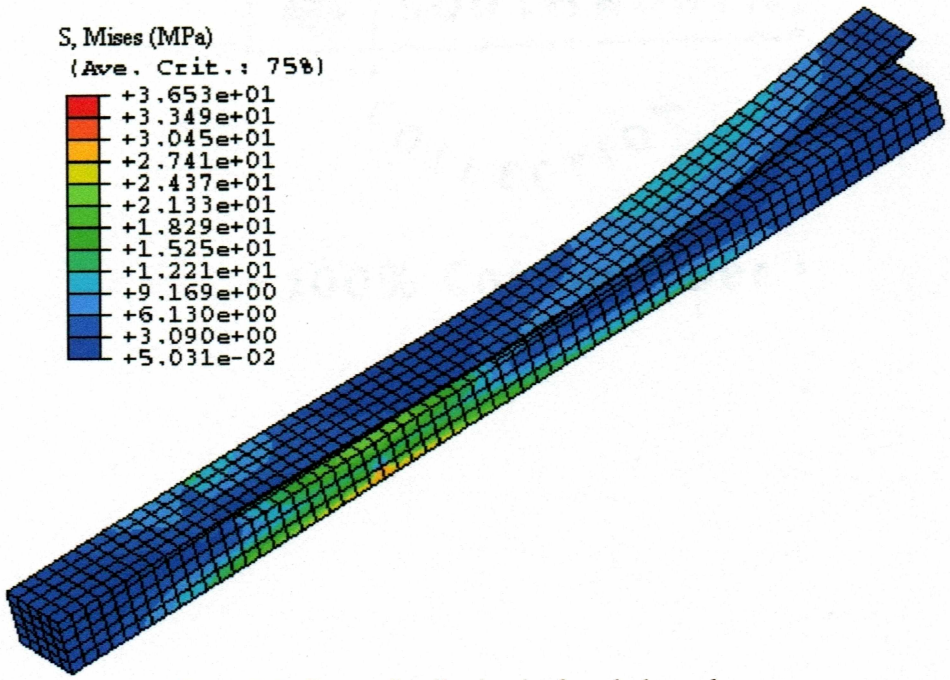

Figure 2.8: Stress distribution in the whole package .

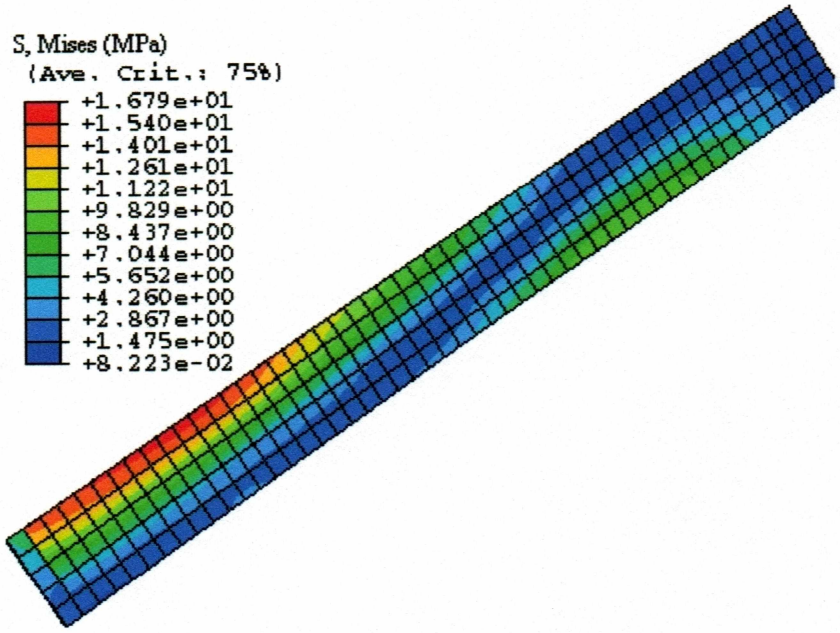

Figure 2.9: Stress distribution in the beam .

Figure 2.10 provides a comparison of stress variation at various points in the beam during the drop test simulation. It is observed that the maximum stress reached is not exactly at the anchor but near to it, as shown in Figure 2.8. This is due to the orientation of the switch during drop.

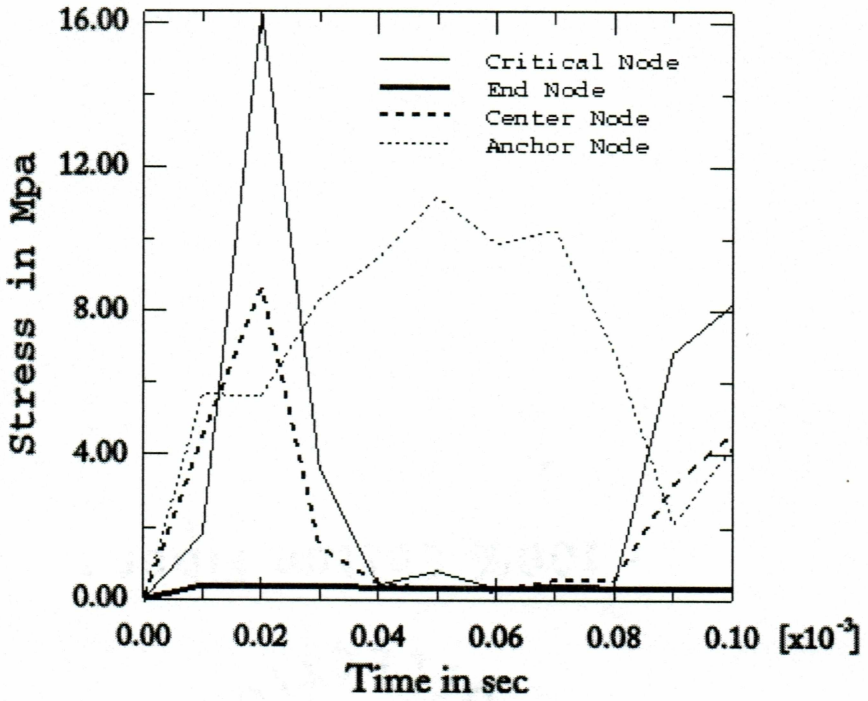

Figure 2.10: Comparison of stress variation at various locations during the drop test .

Figure 2.11 shows the shock levels that various sections of the beam were subjected to during the drop test. The maximum shock obtained was at the anchor and was around 350,000G. Figure 2.12 demonstrates the variation of maximum stress reached at different locations in the beam section for different drop heights. The maximum stress is increasing at an exponential rate with drop height.

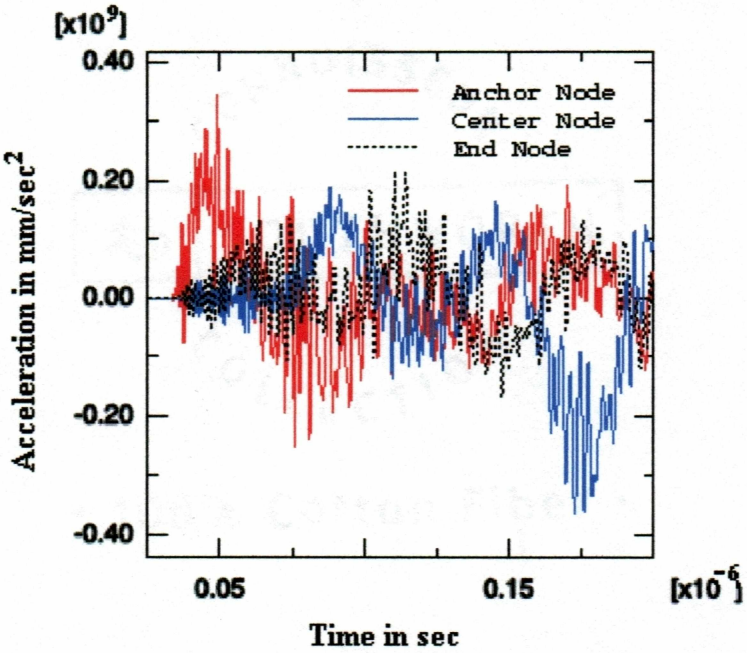

Figure 2.11: Maximum shock produced at various locations

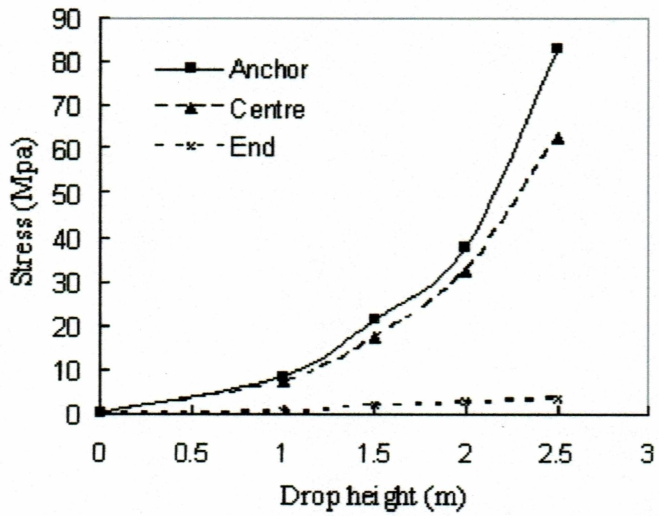

Figure 2.12: Variation of maximum stress at various locations in the beam with drop height .

2.5 Summary

The micro switch considered for the thesis work will have no reliability concerns from the stresses of mechanical shock and cyclic loading. Simulation results have shown that the maximum stresses in the Al switch are relatively smaller than the yield stress for both of the loading conditions. Therefore, the plasticity-related reliability issue will not be a concern. The results are also in good agreement with the recently published experiment results that MEMS switches can operate (on and off) up to 100 billion cycles with no observations of mechanical failure at the anchor where the maximum stresses reside [21], [26]. Hence, the rest of the thesis will focus on the study of the failure modes from the material point of view.

Chapter 3: Electromigration in RF MEMS Switches

In the previous chapter we have seen that the MEMS switch is reliable under mechanical forces like shock and deformation. In this chapter the reliability of the MEMS switch from material point of view is considered. From the literature it was found that most of the MEMS switches under low power applications exhibited up to billion cycles without any failure. When subject to very high current stresses, the failure in MEMS switches was probably due to dielectric charging for capacitive switches and very high temperatures at contacts for resistive MEMS switches. However, the reason behind the failure in medium to high power applications are not well understood [28], 29] and this is still an area under extensive research.

The current densities in MEMS switches for medium to high power applications are very large, which will probably induce electromigration [30]. This fact was found very recently. Although such a possible situation has been addressed by a few authors, no attempt was made so far to study the effect of electromigration on the reliability of MEMS switches. The remaining part of the thesis focuses on investigating the effects of electromigration on the performance of micro-switches.

In this chapter the equations governing electromigration in polycrystalline structures were formulated and a MATLAB program was developed to estimate the lifetime of micro-switches under electromigration. The results presented in this chapter didn't consider the effect of Joule heating on electromigration; the combined effect will be considered in the next chapter. The results were compared with published work passivated metallic strips to validate the program. A few justified assumptions made in the simulations will be discussed in the later sections.

3.1 Brief Review of Electromigration

Electromigration is a mass transport in metal due to the momentum exchange between conducting electrons and diffusing atoms [31-33]. Electromigration is a major failure phenomenon that usually occurs in thin film interconnects when the current density exceeds some threshold value [30], which is about 5×10^5 A/cm^2 for aluminum and gold conductor lines.

The mass transfer (diffusion) is mainly through grain boundaries [32] in a temperature range below 0.5 T_m, where T_m is the melting point of metal. Such mass transport therefore obeys the diffusion equations [33] [34]. However, the driving force here is more complicated than that involved in a pure diffusion process driven by the concentration gradient. The driving force for electromigration consists of the "electron wind force" and the "direct field force". The electron wind force refers to the effect of momentum exchange between the moving electrons and ionic atoms when an electric current is applied. The direction of the electron wind force will be opposite to the direction of the electric field. On the other side, as the ions are positively charged, they tend to move in the direction of the applied electric field. The net effect of these two forces determines the actual direction of movement of atoms. For Au and Al, the electron wind force dominates over the direct field force; the movement of atoms will therefore be in the direction of the electron flow [31], [33]. Hence in Al or Au conductor lines the mass accumulation due to electromigration occurs at the anode side and depletion occurs at cathode side. It was found that the mass accumulation and depletion caused by electromigration in an interconnect produce a stress gradient along the migration paths, as the surrounding material (usually substrate) opposes the formation of hillocks. It results in a compressive stress near the anode side, leading to a global stress gradient between anode and cathode. This stress gradient will oppose the evolution of electromigration mass transport.

When the current is switched off, a back flow of mass will appear in order to relax this stress gradient. This stress induced mass backflow was first observed by Blech [35] [36]. The discussion so far is applicable to thin film interconnects that are usually embedded within a substrate. For the electromigration in RF MEMS switches, which are unpassivated, it is totally a different story. As the current carrying strip of a MEMS switch is free without any surrounding substrate (as in interconnects), nothing could oppose the formation of hillocks. Hence there is no likelihood of the development of stresses. As there are no stresses opposing the diffusion process, the mass backflow (also referred to as relaxation) doesn't exist in this case.

3.2 Equations Governing Electromigration

The following equations [37] are more general and are applicable for any single grain boundary. These equations can be directly applied to bamboo and near bamboo structures where the width of the conductor lines is about a grain size.

The atomic flux J is related to the total driving force F through the diffusion equation:

$$J = \frac{ND}{kT}F = \frac{D}{\Omega kT}F \tag{1}$$

where N is atomic concentration, k is Boltzmann's constant, Ω is the atomic volume, T is the absolute temperature, and D is the atomic diffusion coefficient.

The driving force F is due to the electrical field E and can be generally expressed as a product of electrical field E and an effective ionic charge eZ^*, where e is electronic charge and Z^* is effective charge number, which accounts for the "net effect" of the electron wind force and the direct electrical field force. For the case of an ohmic material, the electric field E is the resistivity (ρ) times the current density (j) i.e., $E = \rho j$

Hence the equation for driving force is:

$$F = EeZ^* = eZ^*\rho j \tag{2}$$

Combining Equations (1) and (2), the final equation for atomic flux is:

$$J = \frac{ND}{kT} eZ^*\rho j \tag{3}$$

It is noted that ρ is temperature dependent and is expressed as:

$$\rho = \rho_0(1+\alpha(T-T_0)) \tag{4}$$

where ρ_0 is the resistivity of film at room temperature T_0, and α is the temperature coefficient of resistivity.

3.3 Governing Equations for Polycrystalline Structures

For a polycrystalline structure the governing equations of electromigration [37-39] will be more complex, as they take in to account, the parameters like the grain misoreintation angles, and the grain boundary inclination angles as illustrated in Figure 3.1.

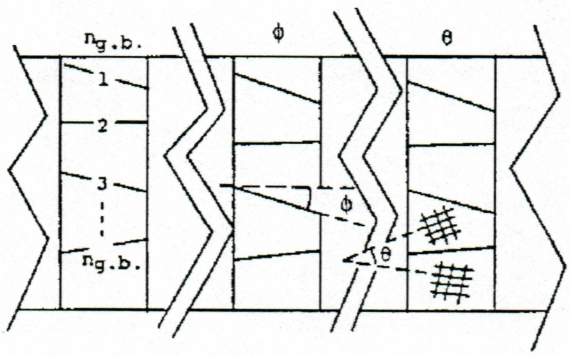

Figure 3.1: Illustration of grains, grain boundaries, grain boundary misorientation-angles, θ's, and inclination angles, ø's. [56]

For a polycrystalline structure, the atomic flux in the i[th] grain boundary is:

$$J_i = \frac{N_i D_i}{K_i T_i} F_i \tag{5}$$

where N_i is atomic concentration at the i[th] grain boundary and $T_i = T(x, y, t)$ is the absolute temperature at the location of that boundary

The diffusion coefficient D_i along a grain boundary is determined by the grain boundary misoreintation angle:

$$D_i = \begin{cases} D_0 \sin\frac{\theta_i}{2} e^{\frac{-Q_0}{kT}} & \text{For } \theta_i \le 37^\circ \quad (6) \\ D_0 \sin\left(\frac{37}{2}\right)^0 e^{\frac{-Q_0}{kT}} & \text{For } 37^\circ < \theta_i \le 60^\circ \quad (7) \end{cases}$$

where D_0 is the pre-factor (about 10^{-4} cm^2/sec for aluminum), and Q_0 is the grain boundary activation energy of the film (about 0.6eV for Al and about 0.9 eV for Au).

The above equations are valid for $0° < \theta \le 120°$ and are symmetric about 60 °. Since Al films are highly oriented along <111> plane, θ can be considered to vary between 0° and 60 ° [49].

Therefore the driving force is given by

$$F_i = eZ^* E \cos\phi_i = eZ^* \rho_0 j[1 + \alpha(T - T_0)]\cos\phi_i \tag{8}$$

Substituting Equations (6), (7) and (8) in Equation (5), we obtain the governing equation for electromigration in polycrystalline structures,

$$J_i = \frac{N_i D_0}{kT} eZ^* \rho_0 [1 + \alpha(T - T_0)] j \cos\phi_i \sin\frac{\theta_i}{2} e^{\frac{-Q_0}{kT}} \tag{9}$$

If considering the healing effects, i.e., the mass back flow due to a stress gradient, the actual mass flux will be less than that in Equation (9). In general, this mass back flow can be replaced by finding the threshold current density j_c, below which electromigration doesn't occur. Below this threshold value, the stress gradient is dominant and opposes the electromigration. Therefore, if we consider this back flow due to the stress gradient, the Equation (9) becomes,

$$J_i = \frac{N_i D_0}{kT} eZ^* \rho_0 [1 + \alpha(T - T_0)](j - j_c) \cos\phi_i \sin\frac{\theta_i}{2} e^{\frac{-Q_0}{kT}} \tag{10}$$

where j_c is the threshold current density.

3.4 Governing Equations for Simulations and the Assumptions

For a polycrystalline structure in a metallic strip, the mass accumulation and depletion do not appear only at the ends of the strip; rather, they occur at every vacancy source and sink pair. These pairs are usually the intersections of the grain boundaries. As a result there exists a local stress gradient between every pair of intersections. The stress field from adjacent intersections is also superposed on this stress field. Thus the exact stress at any point is a superposition of all these stress. In addition, there may be other contributions, like the residual stresses and other external stresses. Since a polycrystalline structure consists of many grain boundary intersections, it may not be numerically efficient to find the stress at every intersection. Usually an averaged threshold current density for the whole conductor strip is chosen for simulations.

In this thesis the effects of this stress gradient is totally neglected so that the threshold value in Equation (10) is zero. This assumption was justified by the following [41]: (1) Unlike interconnects the beam structure in a RF MEMS switch is just suspended without any surrounding materials (like substrate) to refine the formation hillocks for producing a stress gradient; (2) Even if there exists self oxidation on the surface of Al and Au films that may be sufficient to oppose the surface diffusion process, it is not enough to produce a considerable stress gradient, as this thin film of oxide cannot totally oppose the formation of hillocks. In addition MEMS Al switches are usually manufactured in a controlled environment and will be hermetically packaged, which also retards the further formation of thick passive oxide layers over the surface of Al beams.

Thus the governing mass flux equation used in simulations is Equation (9). Instead of calculating the flux through any grain boundary, it would be very useful if we could determine the amount of mass accumulated or depleted at any grain boundary intersection. This can be obtained by finding the mass flux divergence at the intersections.

By defining:

$$\Delta Y = \sum_{i=1}^{n_{gb}} \theta_i \cos \phi_i \tag{11}$$

where $\theta_i = \begin{cases} \sin\dfrac{\theta_i}{2}, & \text{for } \theta_i \leq 37 \\ \sin\dfrac{37}{2}, & \text{for } 37^{\circ} < \theta_i \leq 60^{\circ} \end{cases}$

and where n_{gb} is the number of grain boundaries at an intersection. (The most commonly seen intersection in the microstructure of any material is formed by three boundaries [37]). In practice n_{gb} is taken as 3 for a 2-D poly crystalline structure. Also the grain boundary intersections will be referred as "Triple Junctions" hereafter.

The flux divergence at an intersection is given by,

$$\Delta J = \sum_{i=1}^{n_{gb}} J_i = \frac{N_{gb} D_0}{kT} eZ^* \rho_0 [1 + \alpha(T - T_0)] j \Delta Y e^{\frac{-Q_0}{kT}} \tag{12}$$

It is noted that the threshold current density j_c has been neglected in Equation (12).

Because of this flux divergence, there will be either mass depletion if $\Delta J < 0$ or mass accumulation if $\Delta J > 0$ at each of the triple junctions. As the sign of flux divergence is dependent on ΔY (clear from Equation (12)), the mass depletion or accumulation occurs depending on the sign of ΔY.

The number of atoms accumulated or depleted at an arbitrary intersection over a time period Δt is:

$$\Delta N = \delta h \Delta J \Delta t \tag{13}$$

where δ is the grain boundary width, h is the film thickness, and ΔJ is the flux divergence at the intersection. The rate of the volume change of the mass depleted or accumulated at the triple junction is:

$$\frac{\partial V}{\partial t} = \Omega_0 \frac{\partial (\Delta N)}{\partial t} = \delta h \Omega_0 \Delta J \tag{14}$$

where Ω_0 is the atomic volume.

Equations (12) and (13) are used to simulate the electromigration and calculate the void size.

3.5 Simulation of Electromigration

While simulating electromigration for a polycrystalline structure, the first thing is to generate a geometrical pattern that represents the grain texture of the metal strip under

consideration. A two-dimensional model was considered to simulate the process of electromigration in the strips as the diffusion in the lateral directions of the thin metallic strips is negligible. This two-dimensional modeling assumes that the grain boundaries are parallel to the metal plane. The assumption would be reasonable, since the grain size is larger than the thickness of the Al switch.

Commonly used methods to generate a two dimensional grain structure include the Voronoi Polygon Method, Triple Junction Lattice Method, Stacking Grains method and a Perturbed Hexagonal Grain Structure [37]. In this thesis the Voronoi Polygon Method [40] was employed to produce the microstructure of grains. In this approach, polygons are generated in a random manner as grains in the metal strip. First, the metal strip is divided in to a matrix of small rectangular cells. All the cells are equal in size, which is about the desired average grain size. Then a point is distributed randomly in each cell. These points are considered as the seeds (nuclei). The edges of a polygon are formed by constructing the perpendicular bisectors of rays connecting a given seed and its neighboring seeds. The points enclosing a polygon generated this way form a set of points that are an equal distance from the cell's seed as well as from the seeds of neighboring cells [42]. The distribution of seeds within the cells may be a random, uniform or Poisson distribution. For the simulations in this chapter a random distribution was used. Figure 3.2 shows a microstructure with 6 x 15 units of cells to form an average grain size of 1 unit.

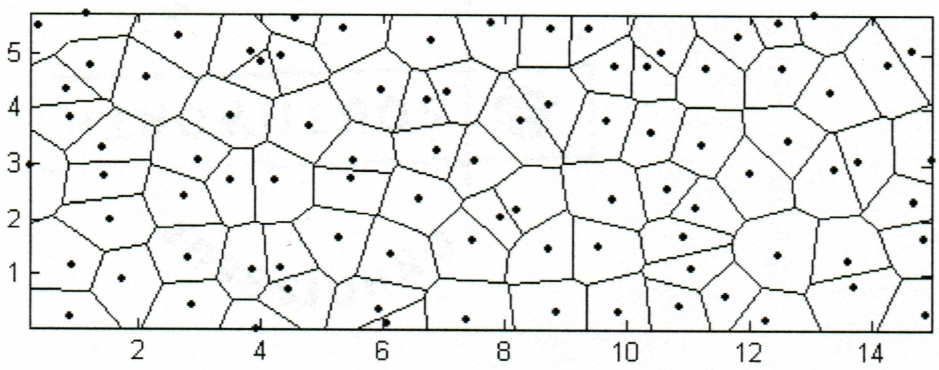

Figure 3.2: A 6μm × 15μm Voronoi structure with 1μm average grain size .

Once the grain texture is generated, the next steps are to simulate the electromigration process and analyze its effect in changing the properties (like resistance, temperature) of the current carrying strip.

The total resistance of the conductor strip will be considerably affected by electromigration degradation. Hence this property will be monitored.

A failure criterion is chosen to stop the simulation. Usually a certain percentage increase in resistance or a certain percentage loss of mass across the conductor line is adopted as a failure criterion [37] [43-44]. In this thesis, to be consistent with the real time operation of the micro-switch, three types of failure criteria were chosen, namely, (1) the percentage increase in resistance when joule heat effects are not considered (as in the simulations in this chapter), (2) reduction in beam width due to formation of voids in time, and (3) the maximum temperature of the beam.

As the electromigration process evolves the shape of the grains changes, it would be over optimistic in predicting higher percentage changes in resistance. The reason is that it's not possible to update the grain shape during the simulations. In addition, these microstructural parameters, like the grain boundary angles, affect electromigration. Due to the above mentioned reasons the results of computer simulations would be only valid until a 5 to 6% change in resistance occurred [32]. Any results presented above this range are under the assumption that the grain boundary angles and other microstructural parameters do not change during electromigration.

While calculating the resistance the model assumes that hillocks have little effect, as they don't divert any current. On the other hand, voids have a major effect on resistance, since the formation of voids reduces the cross-sectional area of the current

To calculate the resistance the strip is discredited in to a finite number of cells equal in size. Each cell is treated as a small resistor; to obtain the total resistance of the strip, the electrical circuit analogy of "Series of Parallel (SP)" or "Parallel of Series (PS)" resistors

is used. For the MEMS beam structure in which the length is much larger than the width, the "series of parallel" circuit analogy was employed in calculating the total resistance of strip. Here all the cells in a column are first treated as a set of parallel resistors and the equivalent resistance of each such column is found. Now each column is considered as a resistor and as these resistors are in series, the total resistance could be found be summing up all the resistances of columns. Figure 3.3 illustrates the concept of SP and PS analogies. In the simulations the cell width of the resistor is taken as the beam width, and hence the total resistance was found by considering that each column is a resistor, and is in series with the adjacent one.

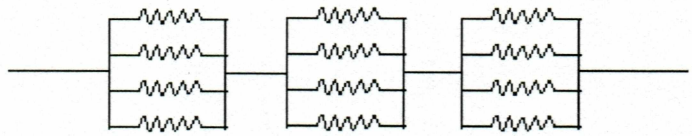

(a) Series of parallel resistors

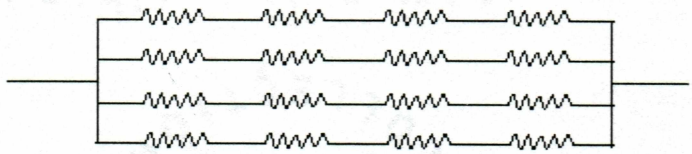

(b) Parallel of series resistors

Figure 3.3: Series of parallel and parallel of series resistors analogies .

The second failure criterion considered is the reduction in width. In the simulation the reduction of the width to half of its original size was treated as failure. Since the results presented in this chapter don't take Joule heating in to effect, the "half melting point" failure criterion is not considered, as the process occurs at a fixed temperature in these simulations. The simulation stops when either of the failure criteria is satisfied. Joule heating effects will be presented in next chapter.

The MATLAB program developed using the procedure explained above is presented in Appendix A. The parameters and contents used in the simulations of Al strips are listed in Table 3.1 as well as in Appendix A.

Table 3.1: Electromigration and diffusion properties of Aluminum .

Parameter	Value
Prefactor (D_0) cm^2/sec	1.0×10^{-4}
Grain boundary activation energy (Q_0) eV	0.6
Effective valence, (Z^*)	1.0
Resistivity at 300 °K (ρ_0)	2.65×10^{-6}
Temperature coeff. of resistivity (α_0) $°K^{-1}$	0.0039

3.6 Results of Simulation

3.6.1 Typical Electromigration Profile until Failure

Figure 3.4 shows the percentage increase in resistance with time for a 20μm × 200μm × 0.5μm Al strip at 400 K.

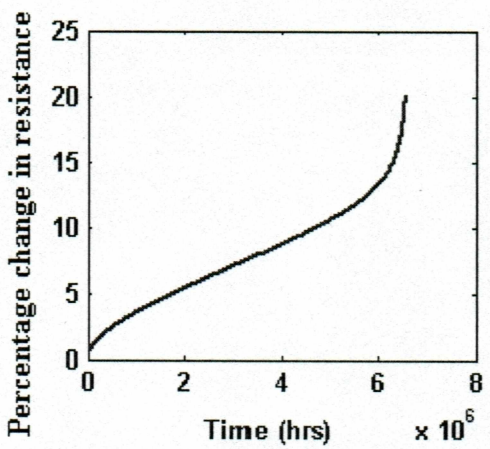

Figure 3.4: Electromigration lifetime profile until failure .

The tendency of the electromigration life profile shown in the figure is consistent with the lifetime profile presented in the works by Harrison *et al.* [45]. The initial current density in this simulation is 3 $\times 10^6$ A/cm^2. The results show a two stage resistance increase: an initial stage of slow increase in resistance followed by a more rapid change leading to catastrophic failure. This two stage resistance change agrees with the common trend observed in the experimental results. This kind of two phase resistance change was first observed by Rosenburg and Berenbaum [46].

At the early stage of electromigration there is a linear relationship between the resistance and time. This linearity has also been observed by many other workers [32] [44-47]. Once the voids start growing the cross-sectional area for the current flow reduces, resulting in increased current densities and resistances at various locations. During the early stage, the resistance slowly increases as the voids grow at a very slow rate. As the electromigration process is directly dependent on the current density, the process will accelerate, resulting in a higher growth rate of voids in a positive feedback manner. This process continues until the voids reach a certain critical size, where the resistance increases at a very high rate leading to failure.

3.6.2 Validation of Model

In order to validate the results, some simulations have been carried out and the results are compared with the experimental data available in literature. Figure 3.5 shows one such comparison. Here the simulation was carried out for an 8.7μm width and 1050μm long polycrystalline Gold line with one micron average grain size. The initial current density in these simulations is 3 $\times 10^6$ A/cm^2, and the temperature 260 °C.

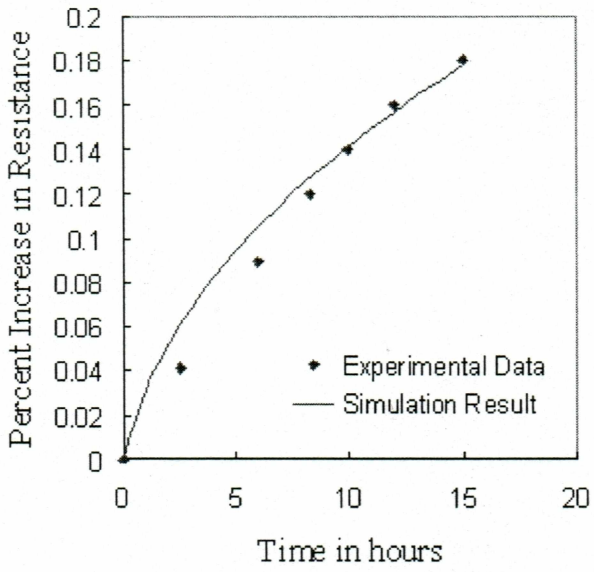

Figure 3.5: Simulation results of percentage change in resistance vs. time compared with experimental data from Tang *et al.*[48].

As shown in the figure, the results are in good agreement with the experimental data. The simulation neglects the effects of current crowding and Joule heating. The small deviation from the experimental values may be attributed to differences in electromigration data used in the simulation, simplification of the model and variations in the microstructure.

3.6.3 Effect of Grain Size on the Electromigration Lifetimes

Figure 3.6 illustrates the effects of average grain size on the failure of the metal strip. The metal strip is the micro-switch cantilever beam made of Al as presented in Chapter 2. The beam is of 200 μm × 20 μm × 0.5 μm. The lifetime was predicted for a 0.5 % change in resistance, i.e., at the early stage of the electromigration evolution, so that the results are more accurate. The simulation was carried out for 1 μm, 1.5 μm, 2 μm, and 2.5 μm average grain sizes. The current density was 3×10^6 A/cm^2 and temperature was kept at 200 °C for all the simulations.

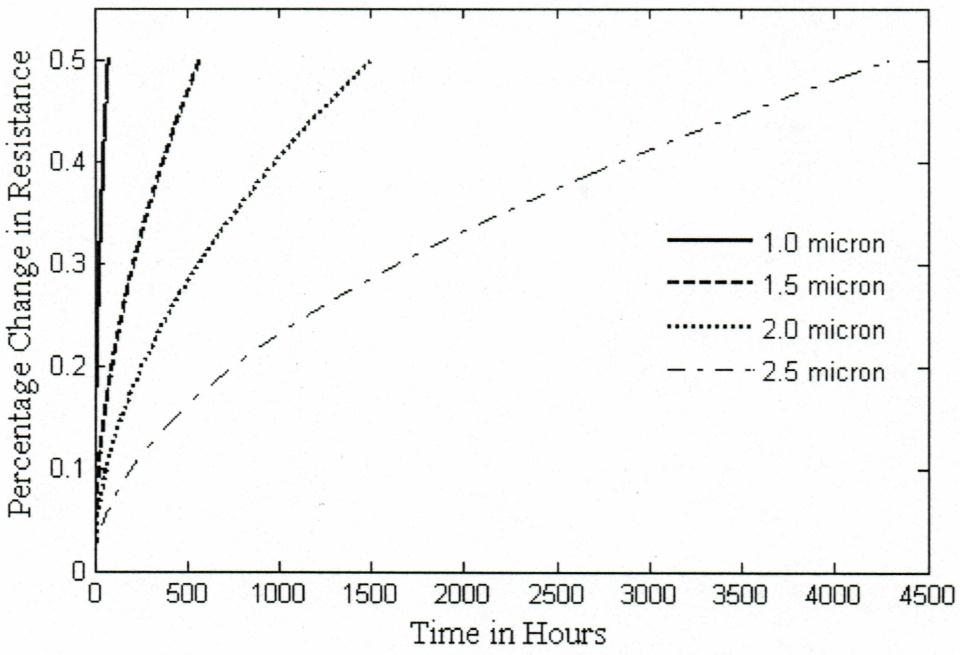

Figure 3.6: Effect of grain size on electromigration lifetime .

The grain size has a great influence on the lifetime of metal strips. As the grain size increases, the lifetime increases. These results are in agreement with the Mean Time to Failure simulations for interconnects by Attardo *et al.* [49]. The increase in lifetime is mainly due to the following reason: a microstructure with larger grains has fewer grain boundaries as well as grain boundary intersections. As these triple junctions are the main sources of flux divergence, fewer negative flux divergence sites result in lower mass depletion and higher lifetime. There is nearly a three times of increase in lifetime for half a micron change in the average grain size. The effect of grain size is similar to that for passivated interconnects.

3.6.4 Effect of Microstructure Variations

The structural factor ΔY in Equation (11) reflects the effects of grain boundaries in the microstructure on the electromigration process and plays an important role in forming the flux divergence. The microstructural parameters that influence the electromigration are

the inclination angle and misorientation angle (Figure 3.1) as mentioned earlier in Section 3.2. As these parameters can be changed in the simulation by changing the positions of distributed seeds during the generation of a Voronoi structure, the effect of these parameters was studied by changing the randomness of distribution and inclination angles. Figure 3.7 illustrates the effect of these microstructural parameters on the electromigration lifetime. The simulation was carried out for the micro switch beam mentioned in Chapter 2.

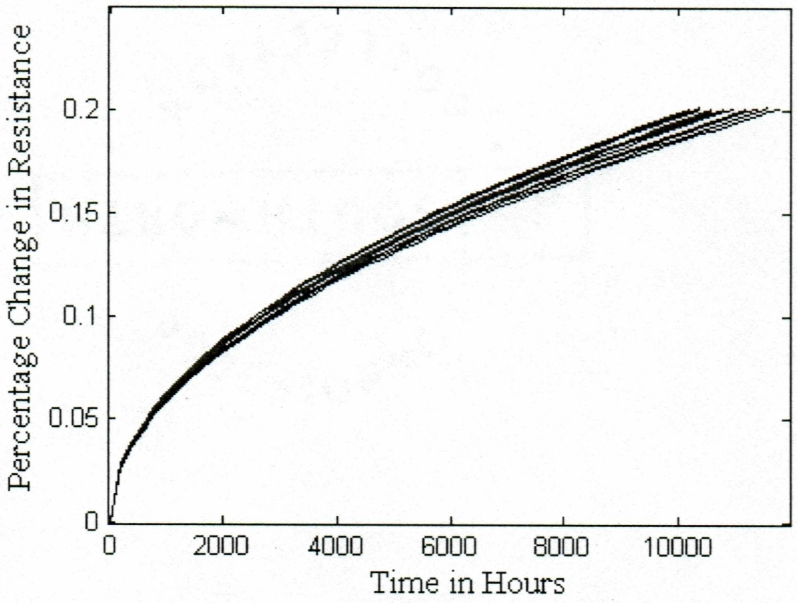

Figure 3.7: Effect of microstructural parameters on electromigration lifetime for 20 different random distributions of seeds in the cells

Figure 3.7 shows the results of 0.2 % resistance change for 20 tests of grain structure generations; i.e., the grain misorientation angles and inclination angles were changed to 20 different values during the simulation. The strip was stressed to 1.3×10^6 A/cm^2 of current at a constant temperature of 400 K. The average grain size was 2 μm for all the tests. It indicates that, as the average grain size remains the same, the microstructure

variations only have a minor influence on the lifetime of a metal strip under electromigration.

3.6.5 Effect of Temperature

The temperature variation on the micro-switch can be the most important factor in accelerating the electromigration degradation, because the atomic diffusion is exponentially dependent on the temperature, as expressed in Equation (6). Figure 3.8 shows the temperature dependence of electromigration in an Al micro switch. The temperatures of the simulated tests are 350 K, 360 K, 370 K, 380 K, 390 K, and 400 K, respectively. The initial current was 1.3×10^6 A/cm^2 and the average grain size was 2 μm for all cases.

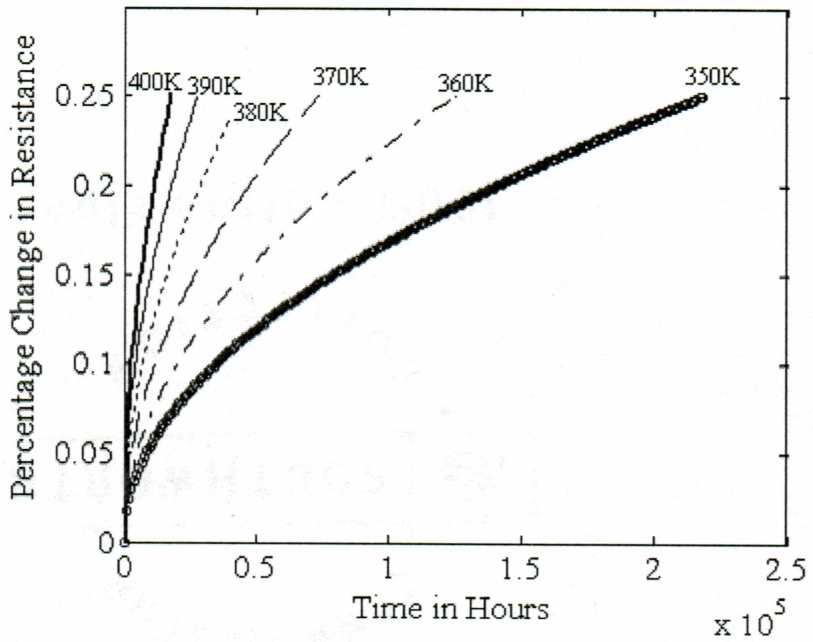

Figure 3.8: Effect of temperature on electromigration lifetime.

The results indicate that even a 10 K rise in temperature can severely affect the lifetime. Table 3.2 summarizes the results from Figure 3.8. Figure 3.9 shows the exponential

dependence of electromigration lifetimes on temperature. Here the base temperature is 350 K.

Table 3.2: Effect of temperature on electromigration lifetime .

Temperature (K)	Lifetime (Hours)	Temperature Rise(K)	Lifetime Reduction	Diffusivity cm^2/sec
350	218000	0	0	2.29148E-13
360	125000	10	93000	3.98667E-13
370	74000	20	144000	6.72389E-13
380	45000	30	173000	1.10327E-13
390	28000	40	190000	1.76489E-13
400	18000	50	200000	2.75771E-12

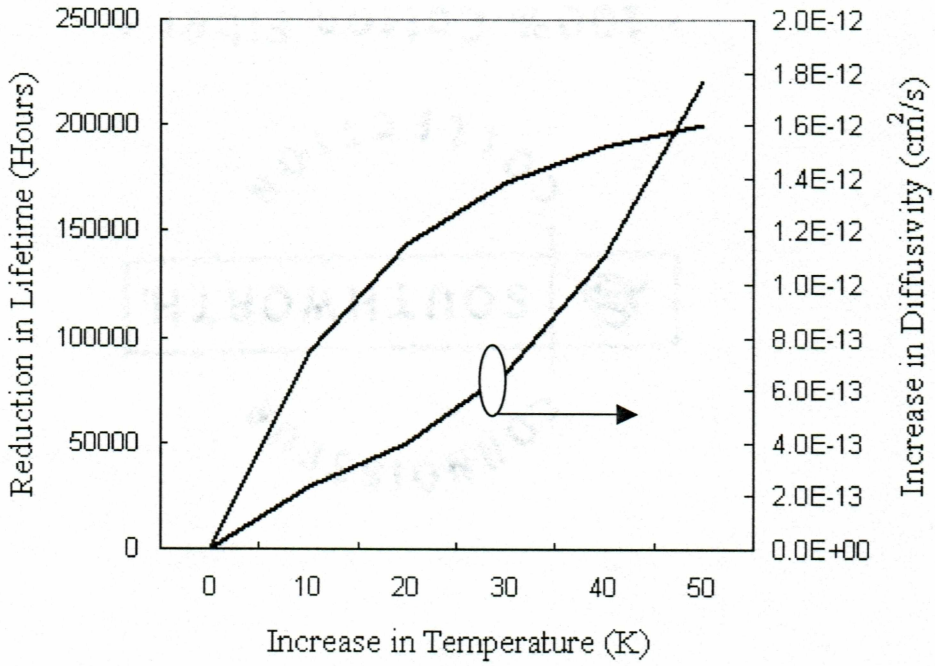

Figure 3.9: Temperature dependence of electromigration lifetime.

It is very clear that temperature has a major impact to the electromigration process and this result raises a reliability concern. As the electromigration progresses the temperature

of the strip will increase dramatically if there is no surrounding material to conduct the heat away. This increase in temperature further accelerates the electromigration, resulting in a positive feedback toward failure.

3.6.6 Effect of Current Density

The current flowing through the conductor is one of the main factors that drives the electromigration. As mentioned earlier in this chapter, the electromigration will not be effective unless the current density (i.e., current flowing per unit cross sectional area) exceeds a certain threshold value. This threshold is 5×10^5 A/cm^2 for Al. As the cross sectional area of a RF MEMS switch is very small, in the range of 10 ~ 100μm^2, even a few milli-amperes of current flow would be sufficient to reach the above mentioned threshold for current density.

The typical magnitude of current for medium to high power application MEMS switches is 100 ~ 350 mA of DC or RF signal current [50]. The cross section of the switch membrane considered is 20 μm × 0.5 μm. The current density in the switch therefore will range from 1×10^6 A/cm^2 to 3.5×10^6 A/cm^2.

Figure 3.10 shows the simulation results for a current density in the range of 1.6×10^6 ~ 3.1×10^6 A/cm^2 (medium to nearly high power application range) using an increment of 0.3×10^6 A/cm^2. The tests were simulated at a constant temperature of 400 K for 0.25 % change in resistance. Comparing the lifetime at 0.25% increase in resistance, when the current density changes from 1.6×10^6 A/cm^2 to 3.1×10^6 A/cm^2, the lifetime varies from 145000 to 75000 hours, i.e., is reduced nearly by half. These results are valid during the early stages of electromigration. At the later stages the lifetime also tends to decrease in an exponential manner, as inferred in Figure 3.4.

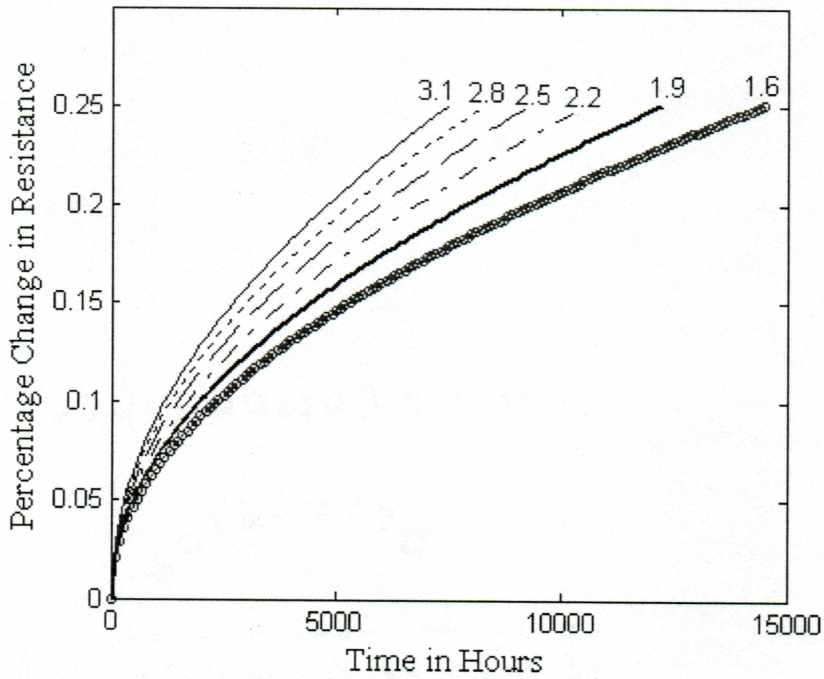

Figure 3.10: Effect of current density (MA/cm^2) on electromigration lifetime

Figure 3.11 summarizes the results from Figure 3.9 at the end of the simulation (at 0.25% increase in resistance).

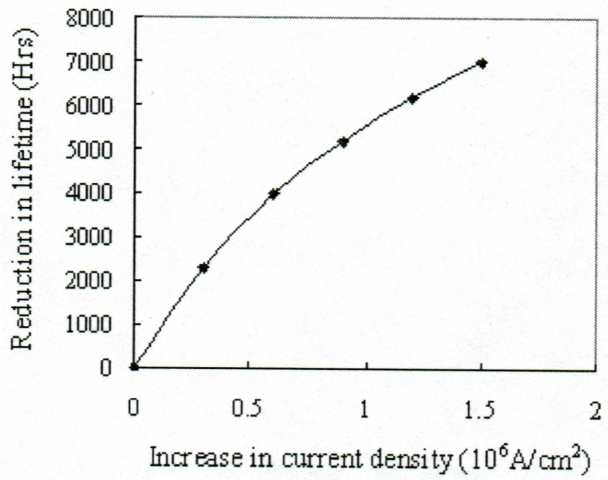

Figure 3.11: Current density dependence of electromigration lifetime.

3.7 Summary

A two dimensional polycrystalline structure resembling the cantilever metal strip of a DC inline contact type RF MEMS switch was generated using Voronoi algorithm. A MATLAB program was developed to simulate the electromigration process. It was found that the major component governing the electromigration degradation is the atomic mass flux divergence at the grain boundary intersections. Since there are many components that govern this mass divergence, parametric study has been performed to understand the effect of each component. Simulating the early stages of electromigration, the Joule heating and current crowding effects are neglected while performing the simulations in this chapter.

The parametric study shows that the microstructural variations like randomness of seed distribution and inclination angles have little influence on the electromigration lifetimes, provided the grain size and cell distribution pattern remain the same. The grain size and temperature were found to be the key contributors in electromigration failure processes. As the grain size increased the lifetime of the switch increased significantly. However, increased temperature reduced the lifetime almost exponentially as expected from the electromigration governing equation. Moreover, the results presented in this chapter provided a good validation for the simulation program. Hence, this program with an integrated Joule heating effect can be used to predict the lifetime of MEMS switches in real time operation.

Chapter 4: Effects of Joule Heating on the Electromigration Reliability of MEMS Switches

Temperature is generally considered as a key parameter in the design of any electronic system. We have seen in the previous chapter that the process of electromigration is exponentially dependent on the temperature. Whenever electrical current passes through a conductor, the temperature of the conductor rises mainly due to resistant heating. This effect of the increase in temperature is called Joule Heating. The reliability of electronic devices depends on how efficiently the heat can be dissipated from the system.

In IC interconnects the electricity is conducted via thin film strips that are in direct contact with substrate, an effective heat sink. Because most of the heat generated in interconnects is conducted away into the encapsulation layer and/or substrate, thin film conductors can usually withstand a current density at least two orders of magnitude greater than traditional bulk wires do. When the current density in a metallic conductor reaches the level of 10^6 A/cm^2, electromigration becomes significant [51], [52].

For passivated interconnects, due to heat dissipation by conduction through the surrounding substrate materials, the temperature rise in the conductors is about 10 °C to 20 °C. However, there exists a major difference of heat dissipation between RF MEMS switches and interconnects [51], [53]. In a MEMS switch the current passes through the micro-strip which is a micro beam suspended in an inert environment (hermetic packages). As current flows, the temperature in the strip increases rapidly to a high value, since there is no surrounding substrate to conduct the heat away. Since the process of electromigration is exponentially dependent on the temperature, the Joule heating will be a major reliability concern in MEMS switches.

Hence the Joule heating effect on the electromigration degradation of MEMS switches was presented in this chapter. A MATLAB program was developed to predict the lifetime of the MEMS switch under combined electromigration and Joule heating.

4.1 Introduction of Joule Heating Effects on Electromigration

Whenever electrical current passes through a conductor its temperature increases due to Joule heating. Joule heating occurs due to thermal resistance loss of energy. The energy loss in terms of Joule heat, Q, depends on the electrical resistance of the conductor and the current flowing in it, which is given by

$$Q = i^2 R \tag{1}$$

where i is the current flowing in the conductor and R is the resistance. Alternatively the energy loss can be expressed as:

$$q = j^2 \rho \quad \text{Watt/cm}^3 \tag{2}$$

where q is heat generated per unit volume, j is the current density (the current flow per unit cross-sectional area), and ρ is the resistivity of the conductor. The resistivity is a property of the material and it is dependent on the temperature:

$$\rho = \rho_0 [\ 1 + \alpha (T - T_0)\ ] \tag{3}$$

where ρ_0 is resistivity of the conductor a at a reference temperature T_0, and α is the thermal coefficient of resistivity (0.0039 $^{\circ}C^{-1}$ for aluminum).

The governing equation of electromigration, one form of the diffusion equation, uses the electron wind force instead of concentration gradient to drive the diffusion process. It can be represented as:

$$J = \frac{ND}{kT} F = \frac{D}{\Omega kT} F \tag{4}$$

where N is the atomic concentration of Al (inverse of the atomic volume Ω), k is the Boltzmann's constant, T is the absolute temperature, and D is the diffusivity. The diffusivity is a parameter exponentially dependent on the temperature and is given by:

$$D = D_0 e^{\left(\frac{-Q_0}{kT}\right)} \tag{5}$$

where D_0 is a pre-factor and is dependent on the material properties, and Q_0 is the activation energy, about 0.5 - 0.6 eV for diffusion along the grain boundaries of Al.

Once the current density in the conductor reaches the threshold value [54], [55] (5×10^5 A/cm^2 for Al and Au), the electromigration will be effective in drifting atoms along the electron flow. Vacancies will be accumulated to form voids and/or nucleation begins and hillocks appear. Since the voids reduce the effective cross-sectional area of the current flow, the local current density increases, resulting in a larger amount of heat generation as given by Equation (2). This increase in heat generation raises the temperature in the strip. The higher temperature in turn accelerates the electromigration process, because of the temperature dependence of diffusivity. This process continues until the voids grow to a critical size, leading to a catastrophic failure of the strips. The whole concept of the thermal accelerated electromigration process can be represented as in Figure 4.1.

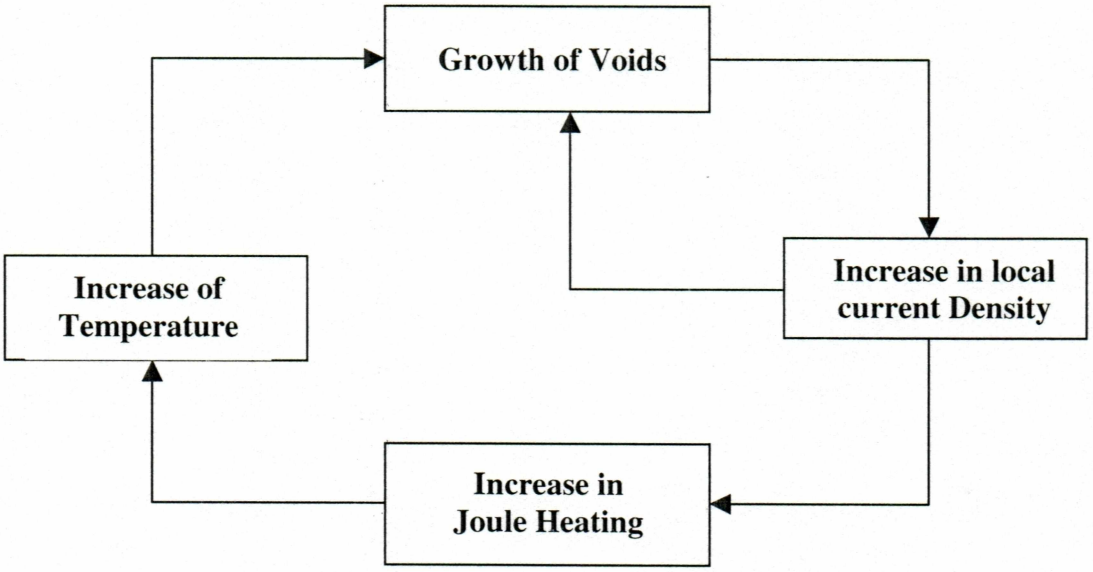

Figure 4.1.Thermally accelerated electromigration, Kiyoshi *et al.* (1981) [56]

The simulation results presented in the previous chapter have neglected the effect of Joule heating. The Joule heating is included in the simulations in this chapter to provide better prediction of the switch lifetime.

4.2 Modeling of Joule Heating

Once the electromigration begins, the heat generated in the strip is dependent on the geometry of the strip, which changes with time. On the other hand, the current distribution also varies with the variation in geometry. Hence, to know the exact temperature distribution in the strip at any time, we may need to solve a transient heat generation model dependent on geometry. This makes the problem not only complicated but also numerically inefficient. Since the results presented in this chapter are for the early stages of electromigration, the temperature distribution follows a steady state [57] during an incremental time.

Simple calculations indicate that the heat dissipation due to both convection and radiation is negligible; the major part is lost through conduction heat transfer. To see this, compare the thermal resistance due to conduction for a point source at the center of the beam:

$$R_{cond} = \frac{l}{4kA} \tag{6}$$

to the convective resistance for an isothermal beam:

$$R_{conv} = \frac{1}{2hlw} \tag{7}$$

In Equation (8), the factor 2 represents an estimate for heat transfer from both the top and the bottom of the beam. For our Al MEMS bridge, which is 200 μm × 20 μm × 0.5 μm, with a thermal conductivity of 237 W/mK, R_{cond} is about 21097 K/W. Assuming a convective heat transfer coefficient of 40 W/m^{2}K [58], [59], R_{conv} is about 3125000 K/W which is about 150 times larger. Hence, the convective heat transfer is expected to be negligible.

Similarly, the heat transfer from the beam due to radiation, assuming the beam to be isothermal is:

$$q = \sigma A \varepsilon (T^4 - T_\infty^4) \tag{8}$$

Where σ is Stefan-Boltzmann constant (5.669 × 10^{-8} W/m^2.K^4), ε is the emissivity, A is the surface area, and T_∞ is the ambient temperature. Assume that the micro strip Al is of black body radiation (i.e., ε is 1 on the top and bottom surfaces of the beam) and the temperature in the beam is half of the melting point (467 K) (at which creep may cause failure), the radiative heat transfer is about 9.0 × 10^{-6} W. Under the same conditions the conduction heat transfer calculated using R_{cond} in Equation (6) is about 8.0 × 10^{-3} W, 1000 times more than that due to radiation. Hence the predominant mode of heat transfer in the switch is conduction.

The steady state-temperature distribution on a rectangular MEMS switch having a length l, width w, and thickness t was obtained using a one dimensional Fourier heat conduction equation with a constant thermal conductivity:

$$k\nabla^2 T = -q \tag{9}$$

where k is the thermal conductivity of the Al switch , and q is the power loss given in Equation (2).

With the current distribution in the beam calculated first, the heat generation at each point can be found using Equation (2). This heat serves as the input to the thermal model in Equation (9).

In order to solve the above equation we need to have two boundary conditions. For the boundary conditions applied to the model, some estimation of the convective and radiative heat transfer magnitudes is required.

Since the heat generated in the beam has conduction paths only towards the ends of beam, and the heat transfer by convection and radiation is negligible, the surfaces of the switch are considered to be adiabatic.

At the left and right ends where the beam is fixed to substrate and in contact with the transmission line, the temperature is prescribed as room temperature or ambient temperature, T_∞ (25 °C). Hence the boundary conditions used to solve Equation (9) are given by:

For the left end x = 0, $T = T_\infty$ (10)

For the right end x = L, $T = T_\infty$ (11)

4.3 Assumptions in the Model

A few assumptions were made in implementing the Joule heating effects on electromigration: (1) The pull-in contact of the micro beam is perfect where the contact resistance is neglected. In practice, this can be achieved by employing proper contact techniques [60] or proper materials like gold and gold alloys. If the contact resistance is very high there will be a considerable amount of heat generated at the contact that makes the problem worse and more complicated. (2) The overall heat generation is calculated by integrating the heat loss density (Equation (2)). The temperature is found by solving a steady-state 1-D Fourier equation, instead of finding a transient solution. This assumption has been commonly used in literature [58], [59], [61] for the thermal modeling of RF MEMS switches. This assumption alleviates the computational burden; however a more accurate solution, solving for the transient state, is still needed.

4.4 Simulation of Electromigration under Joule Heating

Equations (2) and (6) describe the temperature dependence of the electrical properties of the beam. The electrical resistivity varies linearly with the temperature. The facts were embedded in the simulation by implementing the loop in Figure 4.1. Starting with the room temperature (25 °C) and the corresponding resistivity, the temperature is updated based on the heat generation ant any instant. Now the temperature dependent properties in the electromigration governing equation are recalculated for the next time step. This process continues until a failure criterion is met where the simulation stops.

Once the electromigration degradation starts the voids reduce the cross section area for current resulting in high current densities. Hence the heat generated at that section is greater compared to section with no voids. In order to calculate the total heat generation, the switch is divided in to a number of sections and heat generated in each section is calculated based on the cross section and the current density of that section. The overall

heat generation is the summation of heat generated in all the sections. This total heat generated was used in finding the temperature distribution in the beam.

As we are assuming one dimensional heat conduction with adiabatic boundary conditions, the temperature will be maximal at the center of the beam. Nevertheless, in actual practice this is valid for the initial stages of electromigration. Once the voids grow to a considerable size, the temperature distribution will be different. In such situation it is necessary to find the local temperature based on local heat generation and corresponding boundary conditions. Since it is currently infeasible to find the temperature and current distribution based on the varying local geometry in this thesis work, the results presented in this chapter are based on the simplified model discussed so far.

Figure 4.2 summarizes the whole process of electromigration under integrated thermal and electrical modeling in the form of a flow chart.

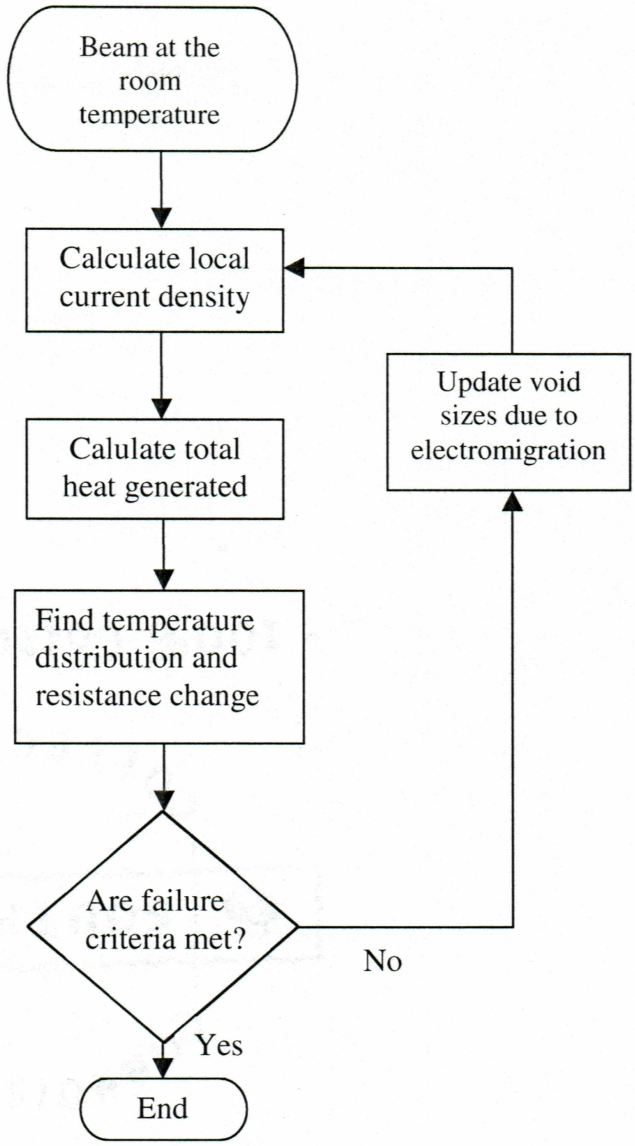

Figure 4.2: Flowchart for simulation of electromigration with Joule heating

For passivated interconnects, hillocks formed in electromigration also play a key role in the failure analysis, as they may extend to the neighboring conduction lines to short the circuit. On the other hand, hillocks in RF MEMS switches are considered to have no effect on the failure, as there is no neighboring conduction line, nor do they divert the current. Hence, only the voids degrade the RF MEMS switch.

As shown in the flowchart Figure 4.2, the simulation stops when a failure criterion is met. Three failure criteria were checked at the end of each iteration: (1) A15 % change in the resistance (2) the reduction of width to half of the original width, and (3) the temperature rise to half of the melting temperature. Many materials, including metals, exhibit creep at temperatures above half the melting point of the material [62]. Hence, an aluminum switch with melting point of about 933 K, is considered likely to fail over time if the temperature exceeds 467 K, which was chosen as the third failure criterion.

While considering the change in resistance the initial resistance is taken as the resistance of the strip at steady state temperature for a given current density, because the geometry of the structure doesn't change during the time this was reached. The results tend to deviate only when there is significant change in the geometry due to void formation. The MATLAB code for simulating the tests of electromigration integrated with thermal modeling is presented in Appendix A.

4.5 Simulation Results

4.5.1 Temperature Convergence with no Electromigration

Figure 4.3 shows the temperature distribution on an aluminum MEMS bridge when no electromigration is occurring. The final converged temperature is the steady state temperature that a switch reaches for a considered current density. Here the test simulation was carried out assuming that there is no electromigration. The final temperature obtained here is due to the Joule heating of the strip for a given current density and it remains constant as long as there is no electromigration or change in geometry.

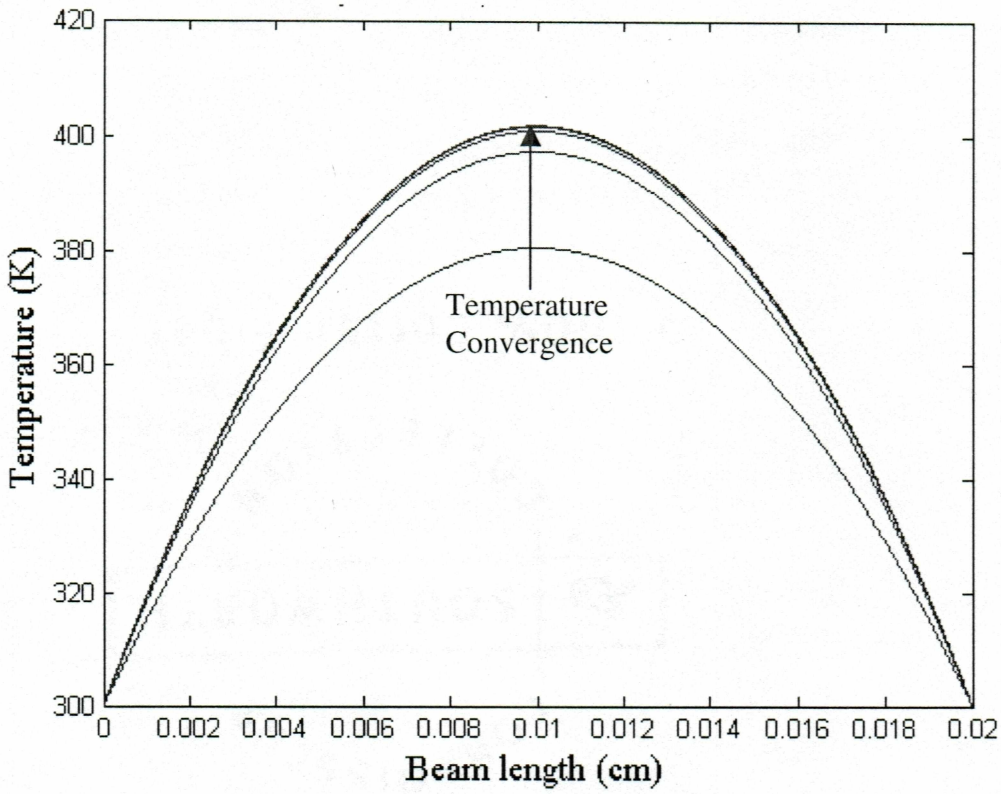

Figure 4.3: Illustration of temperature convergence under the absence of electromigration

The MEMS switch considered here is the same as described in Chapter 2 with 200 μm × 20 μm × 0.5 μm dimensions. The RF current or RMS value of direct current used is 120mA which produces a current density of 1.2×10^6 A/cm^2. The initial temperature of the beam was set at the room temperature, 300K. The simulation stops when the temperature difference between iterations converges to below 0.01%.

In the figure 4.3 the final converged temperature is nearly 401 K which is well below half the melting point of aluminum (467K). This means the temperature of the bridge never reaches half the melting point, indicating no possibility of failure under creep.

The temperature convergence is achieved usually in 4 to 5 iterations. Figure 4.3 shows a large temperature raise followed by little increase later. The reason behind this increase is the temperature dependence of resistivity (Equation (3)). Once the current starts flowing

in the switch, the temperature of the switch raises rapidly because of Joule heating. Now, corresponding to this increased temperature, the resistivity changes. This increased resistivity increases the heat generation (Equation (2)) resulting in a feedback loop toward convergence of the temperature at 401K. However, after two iterations the change in heat generation due to increased resistance and/or vice versa is very little, and the raise in temperature converges to below 0.01%, where the simulation stops.

4.5.2 Temperature Distribution with Joule Heating

Figure 4.6 demonstrates the result of temperature distribution in the MEMS switch with the same initial conditions used in the simulation 4.5.1. Here the Joule heating effect on the electromigration process was taken in to consideration.

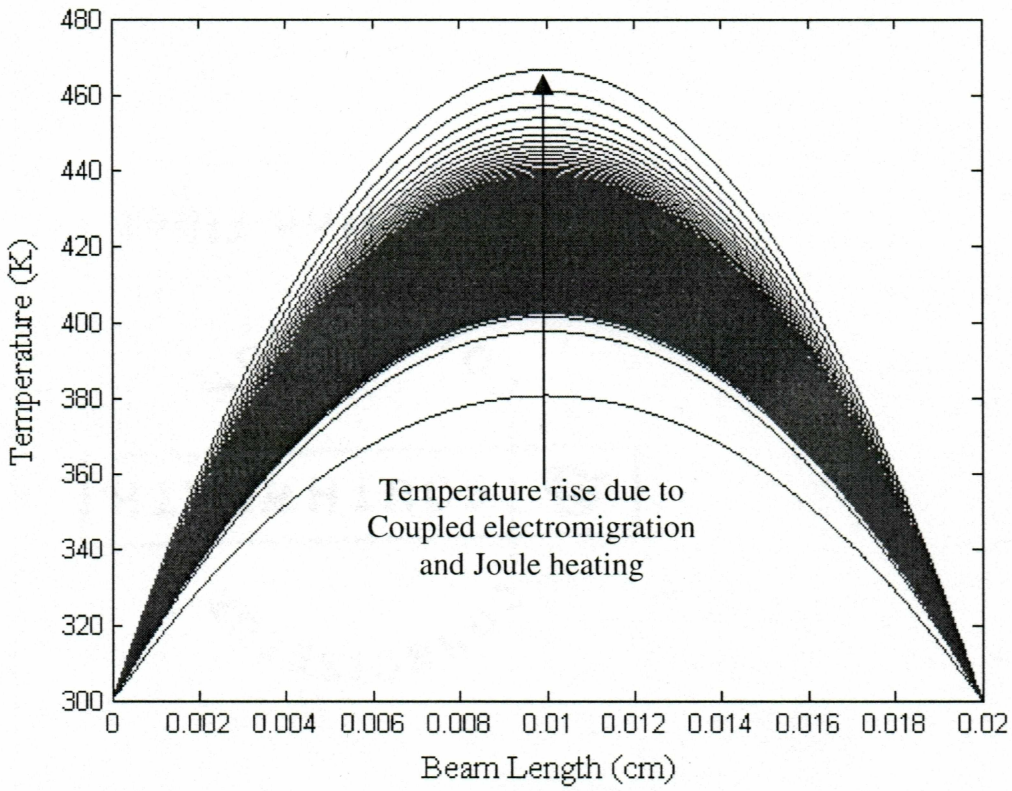

Figure 4.4: Illustration of Joule heating effects on the distribution of steady-state temperature as the electromigration evolves in the MEMS switches.

The temperature in the switch keeps increasing until it reaches the failure criterion (3). This result has significance, as it gives an indication that even in medium to high power applications (10 ~ 40GHz) MEMS switches may fail in time due to the phenomenon of electromigration coupled with Joule heating, and subsequent temperature raise.

Since there are no studies of the electromigration failure possibilities in MEMS switches in literature, this result demands more studies of electromigration related failure. Since the reasons for failure of micro switches in medium to high power applications are not well understood currently, this result may also stand as one of the possible explanations for the failure.

4.5.3 Comparison of Electromigration Life with Joule Heating

In the previous section we have seen that the Joule heating plays a major role in electromigration failures. In order to clearly understand this, the lifetime of the switches were compared with and without Joule heating effects in Figure 4.5. It illustrates the acceleration of the electromigration process under Joule heating. The test for electromigration with Joule heating (top curve) was simulated at 300 K for a stressed current of 1.3×10^6 A/cm^2. Here the beam failed because the voids reached the critical size earlier, due to the Joule heating effect, and the width of the beam reduced to less than half.

The test without Joule heating (bottom curve) was simulated for the same current density at a constant temperature of 400 K. Here the simulation was stopped at the time that the switch Joule heating consideration (top) failed (2,500,000 hours).

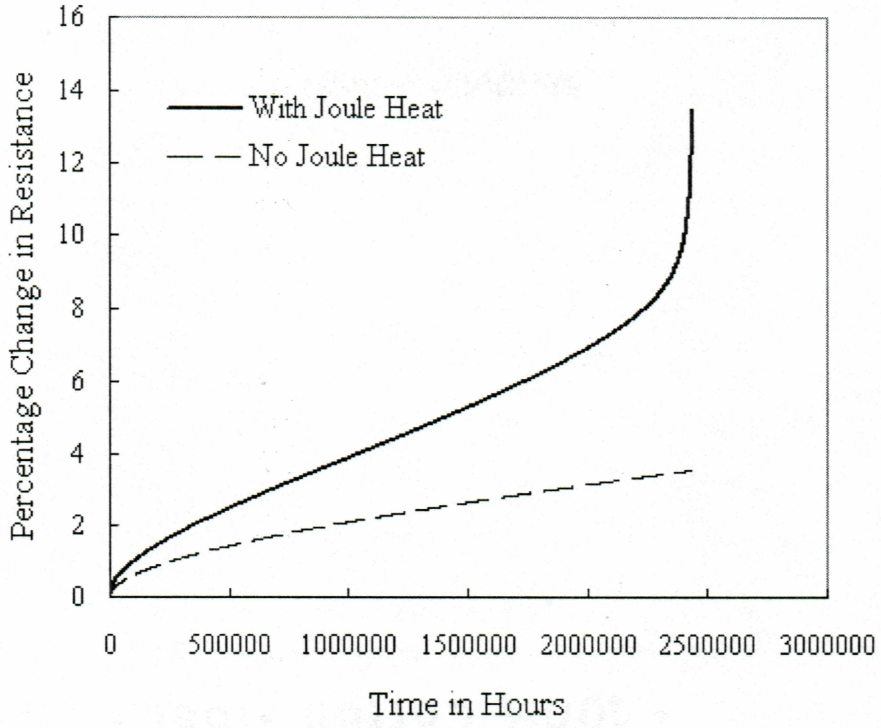

Figure 4.5: Comparison of electromigration lifetimes with and without Joule heating.

The result above clearly indicates the significance of Joule heating in electromigration degradation process. When Joule heating was not considered there was only a 3% increase in resistance during 2,500,000 hours. On the other hand the bridge failed at the same time when the Joule effect was considered.

4.5.4 Electromigration Degradation of MEMS Switches

Figures 4.6 and 4.7 illustrate the void growth in the presence and absence of Joule heating, respectively. Figure 4.6 is for an aluminum strip starting at the room temperature of 300 K and Figure 4.7 is for the same strip under a constant temperature of 400K. The constant temperature in the second case was chosen as 400 K, which is nearly the average of initial and failure temperatures of the first case. In both of the cases the initial current densities are 1.3×10^6 A/cm^2.

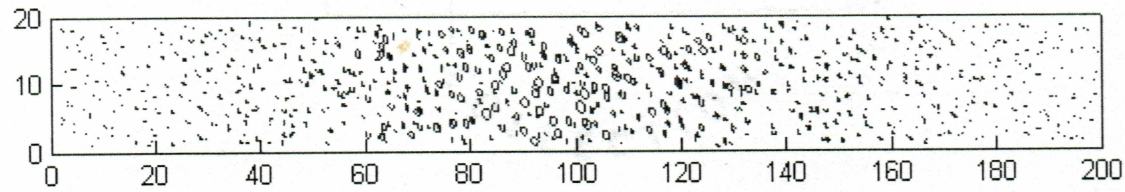

Figure 4.6: Void growth with Joule heating .

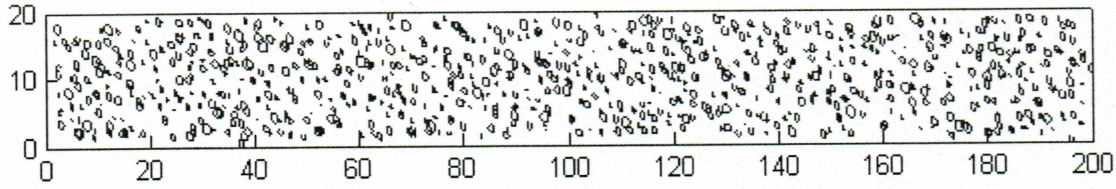

Figure 4.7: Void growth without Joule heating (the temperature is kept at 400 K) .

One can clearly observe the difference in void growth in Figures 4.6 and 4.7. In the first case, where Joule heating was considered, the temperature will be higher at the middle of the beam (Figures 4.3 and 4.4). Hence the void growth rate is also higher near the center and its vicinity compared to the ends, which are assumed to be at the temperature of the substrate (room temperature). In the latter case the temperature was assumed to be same throughout the bridge. Hence the voids are randomly distributed throughout the beam.

4.5.5 Effect of Current Density in Joule Heating Simulations

Figures 4.8 and 4.9 illustrate the effect of current density on the electromigration lifetime while considering the Joule heating. Figure 4.9 was simulated for a resistance change of 1 %. Here the initial current density is 1.3×10^6 A/cm^2 and corresponding lifetime is 48,900 hours. The current density is then increased in steps of 0.2×10^6 A/cm^2 until 1.4×10^6 A/cm^2. Some key differences were observed between the results obtained in the previous chapter where Joule heating was not considered, and the results presented in Figures 4.8 and 4.9 (Joule effect considered).

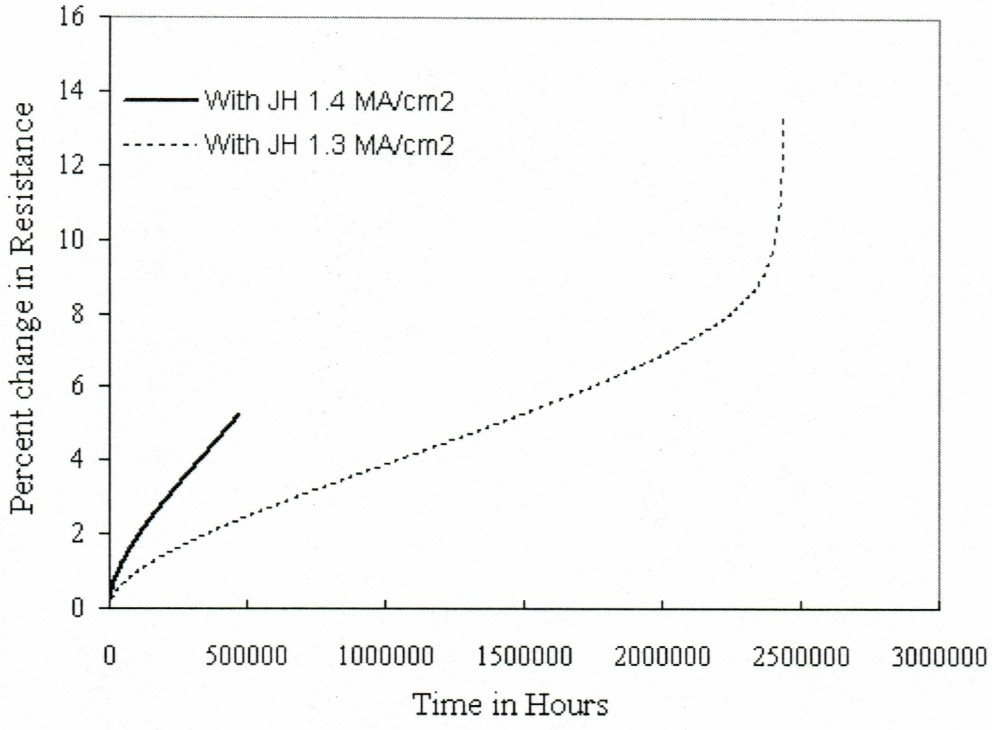

Figure 4.8: Current density effects on electromigration lifetimes .

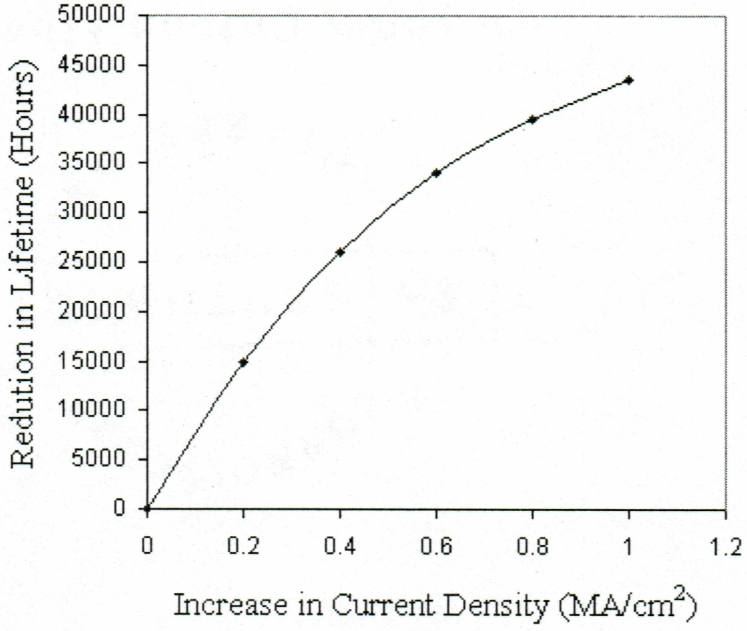

Figure 4.9: Current density dependence of electromigration lifetime .

The first difference is in failure criteria. In the result shown in Figure 4.8 in the plot for 1.3×10^6 A/cm^2 current density (bottom curve),the strip failed because of reduction in the width by one-half. Whereas in the the plot for 1.4×10^6 A/cm^2 (top curve) the strip failed when the temperature of the beam reached half the melting point of aluminum (467 K). In the first case (bottom curve) the voids reached the critical stage and they grew at a rapid rate during the failure stages. In the latter case the temperature of the beam increased at a rapid rate even when voids were below their critical sizes. From this we can say that all the strips subjected to above 1.4×10^6 A/cm^2 would fail due to increased temperature and all the switches subject to below 1.3×10^6 A/cm^2 would fail due to reduction in cross sectional area. However, more simulations with small increments in current densities are required to accurately define these limits.

The second difference is in the rate of change in lifetime. The simulations in Chapter 3 showed a little change in lifetime compared to the change observed in Figure 4.8. In Chapter 3, where there is no Joule heating, an increase of 0.3 MA/cm^2 resulted in a reduction in lifetime by one tenth. Whereas, in the simulation with Joule heating, even an increase of 0.1 MA/cm^2 of current density reduced the lifetime by one-third. Since the reduction in lifetime is very high in this case, it indicates that the current densities are also a major consideration when both Joule heating and electromigration are present.

4.5.6 Effect of Initial Temperature

Figure 4.10 and 4.11 illustrates the influence of switch operating temperature on the electromigration simulations under Joule heating. Both the simulations were stopped when the resistance of the strip increased by 1 %. Figure 4.11 was derived from the simulation results of Figure 4.10. Here the initial temperature is 300 K and the corresponding lifetime is 4,150,000 hours.

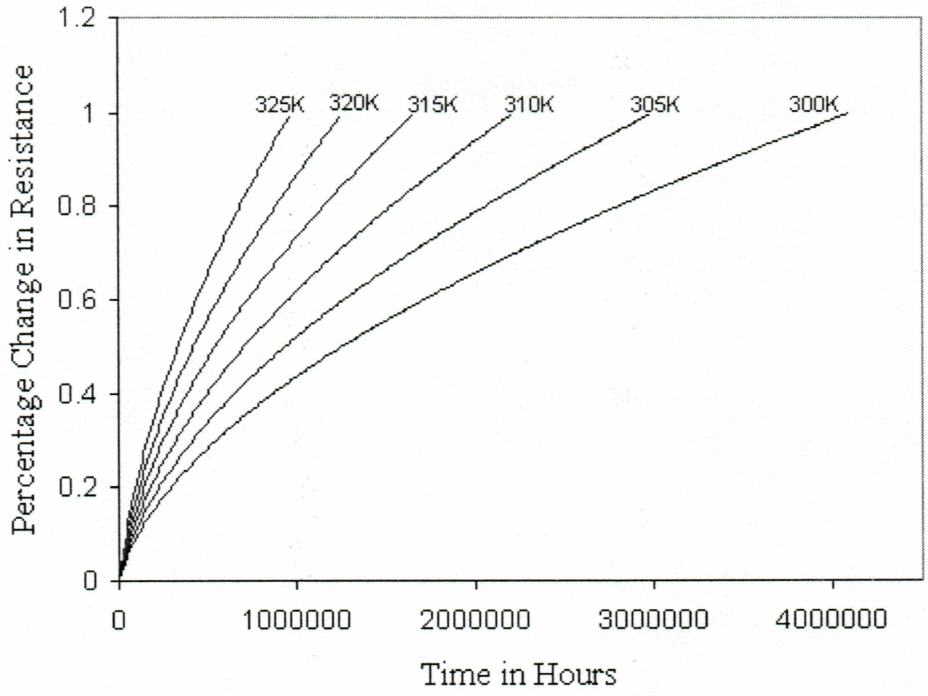

Figure 4.10: Effect on initial temperature on the electromigration simulation with Joule heating.

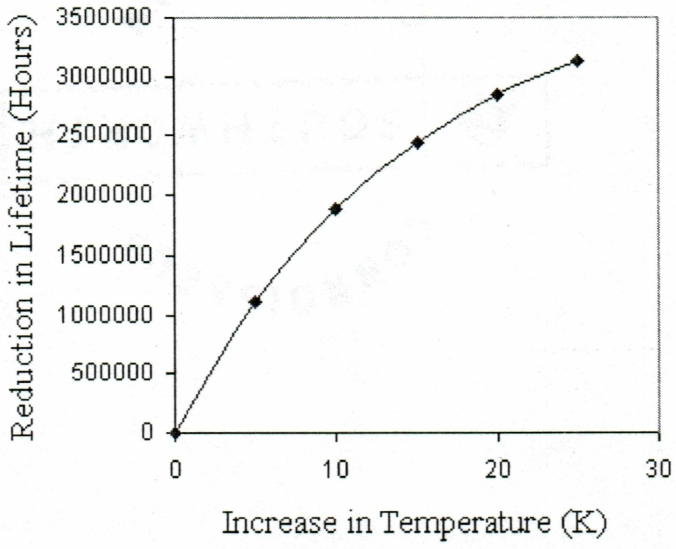

Figure 4.11: Electromigration lifetime dependence on initial temperature.

The results shown in Figure 4.10 and 4.11 indicate a significant influence of temperature on the electromigration lifetime. Even a 5 °C raise in initial temperature has considerably affected the lifetime of the switch.

4.5.7 Electromigration Lifetime of Al vs. Au

Figure 4.12 demonstrates a comparison of the electromigration lifetime between gold and aluminum strips. The tests were simulated for a current density of 1.3 MA/cm^2 and at a temperature of 300 K. Additionally a simulation at 325 K was also carried out for comparison.

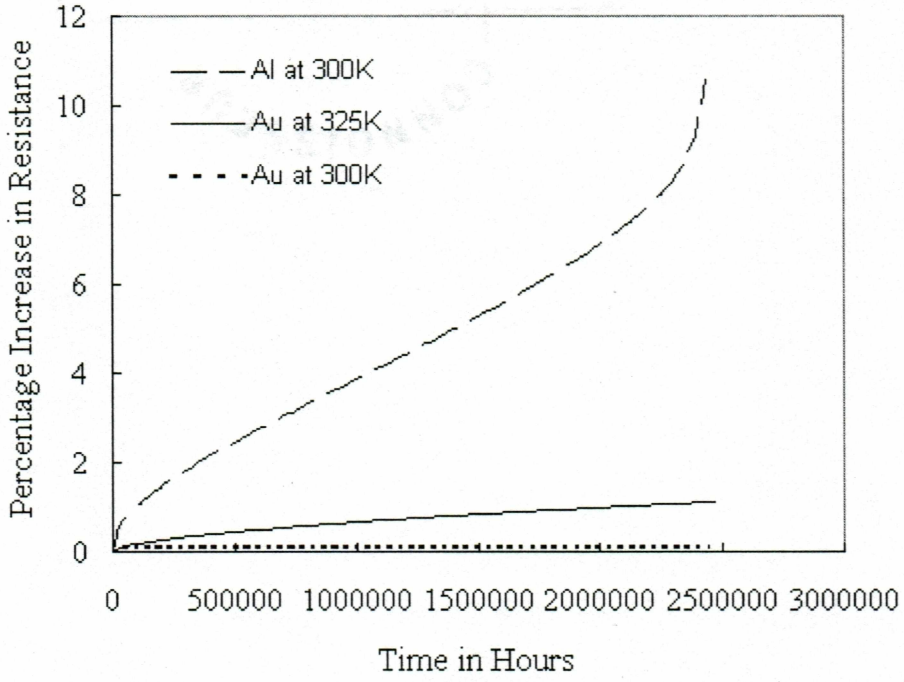

Figure 4.12: Comparison of Al and Au under electromigration

The material properties and electromigration data used in the simulations for Al and Au are provided in Table 4.1.

Table 4.1: Electromigration simulation data for Aluminum and Gold

Property	Aluminum	Gold
Activation energy, (Q_0) eV	0.6	0.9
Thermal conductivity, (K) W/m.°C	237.0	317.0
Resistivity at 300 K, (ρ_0) Ohm-cm	2.65×10^{-6}	2.44×10^{-6}
Thermal coeff. of resistivity, (α) $°C^{-1}$	0.0039	0.003715
Melting point, K	933.0	1337.0
$D_0 \times Z^*$, cm^2/sec	1×10^{-4}	0.4×10^{-6}

The Aluminum strip failed because of the reduced width due to voiding; incidentally, the temperature of the strip reached nearly half the melting point of Al. Meanwhile, the gold strip was still at its initial stages of electromigration. The beam started at 300 K showed only a 0.08 % increase in resistance, whereas the beam started at 325 K showed a 1.121% increase. The simulations for Au strips stopped at this moment for both of the cases. The final temperatures reached are 377 K and 417 K for Au beams started with initial temperatures of 300 K and 325 K respectively. It indicates the temperature reached in Gold is much smaller than that of Aluminum and the void growth in Au is at its beginning stage. This indicates that Gold is superior to Aluminum in electromigration, provided the dimensions and stress conditions are the same.

4.6 Summary

The simulation results demonstrated that the Joule heating has a significant influence on the electromigration lifetime of micro switches. The lifetimes of the switches was nearly halved even for a 10 K rise in the initial temperature of operation

In the literature the thermal simulations on MEMS switches were carried out neglecting electromigration. When such a case was simulated (Figure 4.3), the temperature in the

switch reached a maximum value and remained steady there, without any further increase.

However, when electromigration coupled with Joule heating is considered, the temperature in the switches increased until failure. Since this is a real time scenario, it could be concluded that electromigration is a serious reliability concern for the medium to high power MEMS switches for long term applications.

The results showed that the rate of void formation is more at the regions of high temperature (center of the switch). The simulations for the effect of current density indicated that there exists a value of current density below which the failure of the switches will be due to reduced widths and above which the failure will be due to increased temperatures.

The simulation results also prove that Au is a better option for RF MEMS switches than Al due to its higher melting point and higher grain boundary activation energies. Relatively high lifetimes were observed for Au switches, provided the dimensions and stress conditions are the same. Hence Au could be a good replacement for Al when high reliability is desired.

As the reasons behind the failure of RF MEMS switches for medium power applications are currently not well understood [60], [63], the work presented in this chapter provides a design consideration for reliability.

Chapter 5: Summary, Conclusions and Future Work

5.1 Summary

The reliability of RF MEMS switches has been reviewed. A micro switch, under normal operation, has no reliability concerns due to mechanical shock and fatigue. The finite element analysis in Chapter 2 has verified this by using a single-anchored micro aluminum beam for illustration. However, the reliability due to electromigration has not been studied in the literature. This thesis reports a preliminary study on this topic, to show that electromigration would be a reliability issue. This reliability problem is even more apparent when Joule heating due to electrical resistance of the switch is considered together with electromigration.

Under the presence of a very high current density in the MEMS switch model, electromigration as a mass diffusion phenomenon is likely to happen. Unlike encapsulated interconnects, unpassivated micro switches are in an environment with less capability of thermal conduction and less influence from the back stress and current crowding.

Aluminum has a lower activation energy for mass transport along grain boundaries and on surfaces. In the simulations, the grain boundaries have been taken as the only pathways for mass transport due to electromigration. Due to self-oxidization, the aluminum surfaces can be reasonably neglected as pathways for mass migration.

The resistance change of the micro switch was used to predict the lifetime of the micro switch model under study. Parametric simulations showed that, when the effects of Joule heating are neglected, the average grain size and the temperature are the major factors

that influence the lifetime of the switch under electromigration. Also for the same average size of grains, the variation of the grain structure has minor influence on the electromigration.

When the Joule heating effect is considered, the current density and temperature are the key factors that affect the lifetime of the switch. The thermal model used in simulations only considers heat conduction, since it has been shown (in Chapter 4) that the amount of heat dissipation through convection and radiation are negligible. In this preliminary study, the thermal model was solved using a one-dimensional steady-state Fourier equation. Under the application of a current density with magnitude 1.3×10^6 A/cm^2, the maximum temperature in the micro switch will reach half of the melting point temperature leading toward failure. Due to the mass drifting along the current flow of electrons, voids will be formed in the switch. The simulation results showed that the void distribution is likely more dense near the region of higher temperatures. A test case has been simulated to show that, if the temperature distribution is uniform throughout the switch, the voids are distributed randomly in the switch.

5.2 Conclusions

A few conclusions can be summarized:

1. As the deformation in the switch is very small (about 2 μm), and the magnitude of the actuating force that acts on the switch is also negligible, the strains in the switch never reach the plastic regime to cause permanent deformation.

2. The low stresses obtained in the micro switch even at very high shock levels could be the reason behind their reliability in a vibration environment. The reason for these low stresses may be attributed to the micro scale dimension of the switch.

3. The simulation program developed in MATLAB during this thesis, employing some assumptions about the electromigration and the Joule heating to reduce the computational effort, has qualitatively proved to be a predictive tool for studying the electromigration reliability of RF MEMS switches. The visual illustrations of the degraded structures with void distribution provide understanding of the void growth at any time. One feature of the program is the ability to produce a controllable microstructure of grain distribution for parametric studies of the microstructure effects on the electromigration. From this study, the critical percentage change in resistance was found to be about 10-20 %. More study, however, is needed to accurately determine this critical percentage for failure.

4. The electromigration degradation is a very slow process during the initial stages and shows a linear change in resistance of the strips. As the voids grow to a critical size, the electromigration process accelerates the growth rate of the voids until failure. This stage can be characterized by a rapid increase in resistance.

5. When there is no Joule heating, the temperature and grain size play the key roles influencing the electromigration in the micro switch. The increase in grain size enhances the lifetimes, while increased temperatures diminish the lifetimes of RF MEMS switches. When the Joule heating is included, the current density acts as another major factor to affect the lifetime of the micro switch under electromigration

6. Gold seems to be a good replacement for Aluminum in respect to electromigration reliability. The reliability of Gold in electromigration is better due to (1) a higher grain boundary activation energy (0.9 eV), (2) a higher thermal conductivity (317 W/m °C), and (3) a higher melting point (1337 K). Those factors adversely affect the electromigration evolution.

7. Though the failure lifetime of MEMS switches predicted under the influence of electromigration may not be exact, there are indications from this work that the electromigration phenomenon will definitely play a significant role in affecting the reliability of MEMS switches and is a great reliability concern.

5.3 Suggestions for Future Work

1. More detailed modeling and simulation work are needed to account for the change in the grain boundaries. Also, the temperature distribution modeling in the switches needs to be extended by considering the transient response of heat conduction under a local current density. Finite element modeling may be necessary to improve the models to accomplish the tasks.

2. Experiments may be needed to benchmark the simulations for comprehensive understanding of the electromigration influence on a micro switch.

3. In spite of their superior performance, RF MEMS switches haven't been commercially available for telecommunication and commercial applications due to the high cost of hermetic packaging requirements. Hence packaging solutions for MEMS switches are also an area for future studies.

4. Since the future defense and satellite communication systems demand very high power applications, much beyond 40 GHz and up to 100G Hz frequencies, the electromigration reliability is an area that deserves extensive focus.

References

[1] J. R. Black, "Electron Devices,"*IEEE Transactions*, ED-16, pp.338 (1969).

[2] I. A. Blech, "Electromigration in thin Aluminum films on Titanium Nitride," *Journal of Applied Physics*, Vol. 47(4) (April, 1976).

[3] Black, J. R., "Mass transport of Aluminum by momentum exchange with conducting electrons," Proc., *6th Annual International Reliability Physics Symp.*, pp. 148-159 (1967).

[4] Brian D. Jensen, Kazuhiro Saitou, John L. Volakis, Katsuo Kurabayashi, "Impact of skin effect on thermal behavior of RF MEMS switches," *The 6th ASME-JSME Thermal Engineering Joint Conference* (March 16-20, 2003).

[5] Jad Rizk, Elie Chaiban and Gabriel M. Rebeiz "Steady state thermal analysis and high-power reliability considerations of RF MEMS capacitive switches," *Microwave Symposium Digest, 2002 IEEE MTT-S International* , Vol. 1, pp. 39 –242 (2002).

[6] Brian D. Jensen, Kazuhiro Saitou, John L. Volakis, and Katsuo Kurabayashi," Fully Integrated Electrothermal Multidomain Modeling of RF MEMS Switches", *IEEE Microwave and wireless components letters* , Vol. 13 (9) (September, 2003).

[7] Cheng-fu Chen, Naveen Kishore Karri, and Boris Bracio "Influence of Electromigration on the Reliability of Micro Switches," *The 7th VLSI Packaging Workshop of Japan*, The Westin Miyako, Kyoto, Japan, (Nov. 30 - Dec. 2, 2004).

[8] Vijay K. Vardhan, K. J. Vinoy, K. A. Jose, "RF MEMS and their Applications," John Wiley & Sons, Ltd, pp.109-182 (2002).

[9] Gabriel M. Rebeiz, "RF MEMS Theory, Design, and Technology," John Wiley & Sons, Inc., pp. 1-20 (2003).

[10] Ms. Joanne Wellman, "RF MEMS Switches – General Reliability Concerns," <http://nepp.nasa.gov /index_nasa.cfm/816/. >(21 May, 2004).

[11] Gabriel M. Rebeiz "RF MEMS Switch: Status of the Technology," *the 12th International Conference on Solid State Sensors, Actuators and Microsystems*, Boston, (June 8-12, 2003).

[12] Dr. Michael Cohn, <www.microassembly.com> (2003).

[13] Teravicta Technologies, Inc, Austin, Texas, <www.teravicta.com> (2003).

[14] Danelle M. Tanner, Jeremy A. Walraven, Karen S. Helgesen, Lloyd W. Irwin, Danny L. Gregory, John R. Stake, and Norman F. Smith, "MEMS Reliability in a Vibration Environment," *IEEE International Reliability Physics Symposium*, San Jose, CA, pp.139-145 (April 10-13, 2000).

[15] Valluri Rao, "MEMS Technology with a Focus on Packaging, Assembly and Manufacturing," Presentation, Intel Corporation, http://www.intel.com/research/silicon /mems.htm (September 24, 2002).

[16] Danelle M. Tanner, Jeremy A. Walraven, Karen S. Helgesen, Lloyd W. Irwin, Danny L. Gregory, John R. Stake, and Norman F. Smith, "MEMS Reliability in Shock Environments," *IEEE International Reliability Physics Symposium*, San Jose, CA, pp.129-138 (April 10-13, 2000).

[17] Lei L. Mercado, Shun-Meen Kuo, Tien-Yu Tom Lee, Lianjun Liu, "A Mechanical Approach to Overcome RF MEMS Switch Stiction Problem," *Electronic Components and Technology Conference*, Proc.53 (2003).

[18] G. Blaise and C. Le Gressus, "Dielectric Relaxation Processes and Breakdown of Oxides," in IEEE 1990 Annual Report: *Conference on Electrical Insulation and Dielectric Phenomena*, New York, pp. 231-236 (October, 1990).

[19] A. Teverovsky, A. Sharma, "Analysis of Failure Modes and Mechanisms in Thermally Actuated Micromachined Relays for Harsh Environment Space Applications," *Symposium on Design, Test, Integration, and Packaging of MEMS and MOEMS*, Napoule (2003).

[20] J .R. Reid, "Dielectric Charging effects on Capacitive MEMS Actuators," *IEEE MTT-S International Microwave Svmposium*, RF MEMS Workshop, Phoenix, AZ (May 2001).

[22] MEMSCAP Inc., Sanjose, CA, <www.memscap.com>.

[22]Gabriel M. Rebeiz, N. Scott Barker, Jermy B. Mauldavin, and Guan-Leng Tan "*Mechanical Modeling of MEMS Devices,*" RF MEMS Theory, Design, and Technology, John Wiley & Sons, Inc., pp. 21-57 (2003)

[23] Dimitrios Peroulis, Sergio P. Pacheco, Kamal Sarabandi, and Linda P. B. Katehi, "Electromechanical Considerations in Developing Low-Voltage RF MEMS Switches," *IEEE Transactions on Miocrowave Theory and Techniques*, Vol. 51 (1) (January, 2003).

[24] J. A. Wert, http://www.tu-darmstadt.de/fb/ms/student/fs/german/lab/w5/mse5-0.htm (October 11, 2004)

[25] S. Pacheco, L. P. B. Katehi, C. T. Nguyen, "Design of Low Actuation Voltage RF MEMS Switch," *IEEE International Microwave Symposium Digest*, Vol.1, pp. 165-168 (June, 2000).

[26] S. Majumder, J. Lampen, R. Morrison and J. Maciel, "*An Electrostatically Actuated Broadband MEMS Switch,*" <http://www.radantmems.com> (2004).

[27] C. Wheeler, "*MagLatch ™: the Superior RF Switch Technology Part I – the Advantages of MEMS*", <http://www.securitech.com> (2004).

[28] Gabriel M. Rebeiz, "RF MEMS Theory, Design, and Technology," John Wiley & Sons, Inc., 217 (2003).

[29] Ms. Joanne Wellman, "RF MEMS Switches - General Reliability Concerns," <http://nepp.nasa.gov/index_nasa.cfm/816/> (May, 2004).

[30] I.A.Blech, "Electromigration in Thin Aluminum films on Titanium Nitride," *Journal of Applied Physics*, Volume 47 (4), pp. 1203-1208 (April, 1976).

[31] Richard S. Sorbello, "Theory of the Direct Force in Electromigration," *Physics Review B*, Vol. 25 (8), 5188 (1982).

[32] Pin Fang Tang, "Modeling of Electromigration with Applications to Au on GaAs", Ph.d Dissertation, Carnegie Mellon University (April, 1990).

[33] R. V. Hesketh, "Electromigration: The Electron Wind," *Physics Review B*, Vol. 19 (4), 1727 (1979).

[34] R. P Gupta, Theory of Electromigration in Noble and Transition Metals," *Physics Review B*, Vol. 25 (8), 5188 (1982).

[35] I. A. Blech, "Electromigration in Thin Aluminum Films on Titanium Nitride," *Journal of Applied Physics*, Vol. 47 (4), pp. 1203-1208 (April, 1976).

[36] I. A. Blech and Conyers Herring, "Stress Generation by Electromigration," *Applied Physics Letters*, Vol. 29 (3), pp. 131-133 (1 August, 1976).

[37] Aris Christou, "*Electromigration and Electronic Device Degradation*," John Wiley & Sons Inc., pp 27-77 (1994).

[38] Daniel Young and Aris Christou, "Failure Mechanism Models for Electromigration", *IEEE Transactions on Reliability*, Vol. 43 (2) (June, 1994).

[39] Oliver Kaft, Eduard Arzt, Cynthia A. Volkert, Paul S. Ho and Hidekauz Okabayashi, "Stress Induced Phenomenon in Metallization- Fifth International Workshop Stuggart, Germany 1999," American Institute of Physics Publication (1999).

[40] Franz Aurenhammer, <http://www.voronoi.com/applications> (2004)

[41] K. N. Tu, "Recent Advances on Electromigration in Very-Large-Scale-Integration of Interconnects," *Journal of Applied Physics*, Vol. 94 (9), pp. 5451-5473 (1 November, 2004).

[42] Paul J. Marcoux, Paul P. Merchant, Valdimir Naroditsky, and Wulf D. Rehder, " A New 2-D Simulation Model for Electromigration", *Hewlett Packard Journal*, pp 79 - 84 (June, 1989).

[43] Jun-Cheng Andy Huang, Wei-Ting Kary Chien, and Charles Hung-Jia Huang, "Some Practical Concerns on Isothermal Electromigration Tests," *IEEE Transactions on Semiconductor Manufacturing*, Vol.14 (4) (November, 2001).

[44] R. W. Pasco, J. A. Schwartz, "Temperature Ramp Resistance Analysis to Characterize Electromigration," *Solid State Electronics*, Vol. 26 (5), pp. 445-452 (1983).

[45] James W. Harrison Jr., "A Simulation Model for Electromigration in Fine-line Metallization of Integrated Circuits due to Repetitive Pulsed Currents", *IEEE Transactions on Electron devices*, Vol. 35 (12), 2170 (1988).

[46] R. Rosenburg and L. Berenbaum, "Resistance Monitoring and Effects of Nonadhesion during Electromigration in Aluminum Films," *Applied Physics Letters*, Vol 12 (5), 201 (1985).

[47] Donald J. LaCombe and Earl Parks, "A Study of Resistance Variation During Electromigration in Aluminum Films," *IEEE International Reliability Physics Symposium*, Vol. CH2113-9, pp. 74-80 (1985)

[48] P. F. Tang, A.G. Milnes, C. L. Bauer, and S. Mahajan, "Electromigration in Thin Films of Au on GaAs," *Materials Research Society Proceedings*, Vol. 167, 341 (1990).

[49] M. J. Attardo, R. Rutledge, and R. C. Jack "Statistical Metallurgical Model for Electromigration failure in Aluminum Thin-film Conductors," *Journal of Applied Physics*, Vol. 42 (11), 4343 (1971).

[50] Gabriel M. Rebeiz and Guan-Leng Tan, "*MEMS Switch Reliability and Power Handling,*" RF MEMS theory Design and Technology, Wiley Interscience, pp. 184-219 (2003).

[51] K. N. Tu, "Recent Advances on Electromigration in Very Large Scale Integration of Interconnects," *Journal of Applied Physics*, Vol. 94 (9), pp. 5451-5473 (1 Nov, 2003)

[52] Paul S. Ho, Thomas Kwok, "Electromigration in Metals," *The Institute of Physics*, Vol. 52, pp. 301-348 (1989).

[53] Cheng-fu Chen, Naveen Kishore Karri, and Boris R. Bracio "Influence of Electromigration on the Reliability of Micro Switches," *The 7th VLSI Packaging Workshop of Japan*, The Westin Miyako, Kyoto, Japan (Nov. 30 - Dec. 2, 2004).

[54] E. Kinsbron, I. A. Blech, and Komem, "The Threshold Current Density and Incubation Time to Electromigration in Gold Films," *Thin Solid Films*, Vol. 46, 139 (1977).

[55] H. U. Schreiber, "Electromigration Threshold in Aluminum Films," *Solid State Electronics*, Vol. 28 (6), 617 (1985).

[56] Kiyoshi Nikawa, "Monte Carlo Calculations based on Generalized Electromigration Failure Model," *IEEE International Reliability Physics Symposium*, Vol. CH1619-6, 175 (1981).

[57] Michael Pecht and Pradeep Lall, "Temperature Dependencies on Electromigration," *Electromigration and Electronic Device Degradation*, John Wiley and Sons, Inc., pp. 79-104 (1994).

[58] Brian D. Jensen, Kazuhiro Saitou, John L. Volakis, and Katsuo Kurabayashi, "Impact of Skin Effect on the Thermal Behavior of RF MEMS Switches," *The 6th ASME-JSME Thermal Engineering Joint Conference* (March 16-20, 2003).

[59] Brian D. Jensen, Kazuhiro Saitou, John L. Volakis, and Katsuo Kurabayashi, "Fully Integrated Electrothermal Multidomain Modeling of RF MEMS Switches," *IEEE Microwave and Wireless Components Letters*, Vol.13, No.9, pp. 1-7 (Sept., 2003).

[60] Dimitrios Peroulis, Kamal Sarabandi, and Linda P. B. Katehi, "Low Contact Resistance Series MEMS Switches," *IEEE MTT-S International*, pp. 223-226 (June, 2002).

[61] Gabriel M. Rebeiz, Guan-Leng Tan, "RF MEMS Switch Reliability and Power Handling," *RF MEMS Theory, Design, and Technology*, John Wiley & Sons, Inc. (2003).

[62] Craig R. Barrett, William D. Nix and Alan S. Tetelman, "*The Principles of Engineering Materials*," Englewood Cliffs, New Jersey, Prentice-Hall, Inc. (1973).

[63] Joanne Wellman, "RF MEMS Switches – General Reliability Concerns", <http://nepp.nasa.gov/index_nasa.cfm/811> (21 May, 2004).

APPENDIX A

Table A.1. Electromigration data and the properties of aluminum used in the simulations.

Parameter	Units	Value
Atomic volume (Ω_0)	cm^3	1.7×10^{-23}
Prefactor (D_0)	cm^2/sec	1.0×10^{-4}
Grain boundary activation energy (Q_0)	eV	0.6
Effective valence, (Z^*)	--	1.0
Resistivity at 300 °K (ρ_0)	Ohm-cm	2.65×10^{-6}
Temperature coeff. of resistivity (α_0)	K^{-1}	0.0039
Thermal conductivity (k)	W/cm.K	2.37
Boltzmann constant(K)	J/K	1.3807×10^{-23}

A.2. MATLAB code used in the simulations of electromigration process

```
% PROGRAM TO SIMULATE ELECTROMIGRTION DEGRADATION PROCESS © KISHORE


StratTime=cputime;
%=====================================================================
% CODE TO GENERATE GRAIN-BOUNDARY NETWORKS IN A STRIP OF REQUIRED
% DIMENSIONS 200 x 20
%=====================================================================

X = [];
Y = [];

X_length =100;  % 100 grains of average size = Grainsz
Y_width  =10;   % 10 grains of average size  = Grainsz
GrainSz =2;

rand('state' ,5);
for i =1:X_length
 for j=1:Y_width
     X=[X i-1+rand];
 end
end

for i=1:X_length
  for j=1:Y_width
   Y=[Y j-1+rand];
  end
end
 X=X*GrainSz;
 Y=Y*GrainSz;
%=====================================================================
% DRAW AND STORE THE VERTICES OF GRAIN BOUNDARIES
%=====================================================================
voronoi(X,Y,'-');
[VX, VY]= voronoi(X(:),Y(:));

   tvx=VX;
   tvy=VY;
%=====================================================================
FINDING THE TOTAL NUBMER OF TRIPLE JUCNTIONS AND CORRESPONDING VERTICES
%=====================================================================
   xlist=[VX(1,:) VX(2,:)];
   ylist=[VY(1,:) VY(2,:)];

   clear VX,VY;
   noTriB=0;
   TRIBS=[];
   column=[];
   listodel=[];
```

```
for I=1:size(xlist,2)
           if(xlist(I)~=999);
            tempx=xlist(I);
            tempy=ylist(I);
           else
            continue;
           end

count=0;

         for j=1:size(tvx,2)
              if(tvx(1,j)==tempx) & (tvy(1,j)==tempy)
                  count=count+1;
                  column=[column j];
              end
              if(tvx(2,j)==tempx) & (tvy(2,j)==tempy)
                  count=count+1;
                  column=[column j];
              end
         end

              if count ==3
                noTriB= noTriB+1;

                TRIBS(noTriB,1)=tvx(1,column(1));
                TRIBS(noTriB,2)=tvx(2,column(1));
                TRIBS(noTriB,3)=tvy(1,column(1));
                TRIBS(noTriB,4)=tvy(2,column(1));
                TRIBS(noTriB,5)=tvx(1,column(2));
                TRIBS(noTriB,6)=tvx(2,column(2));
                TRIBS(noTriB,7)=tvy(1,column(2));
                TRIBS(noTriB,8)=tvy(2,column(2));
                TRIBS(noTriB,9)=tvx(1,column(3));
                TRIBS(noTriB,10)=tvx(2,column(3));
                TRIBS(noTriB,11)=tvy(1,column(3));
                TRIBS(noTriB,12)=tvy(2,column(3));

for k=1:3
if (xlist(column(k)) == tempx)
listodel=[listodel column(k)];
elseif(xlist(size(tvx,2)+column(k)) == tempx)
listodel=[listodel size(tvx,2)+column(k)];
else ;
end
end
xlist(listodel)=999;
ylist(listodel)=999;
listodel=[];
end
column=[];
end
```

```
%=========================================================================
% extracting triple junction vertices and the three boundaries vertices
% from TRIBS
 =========================================================================
   tjvs=[];

 for k=1:noTriB

      aray=[TRIBS(k,:)];
      cnt=0;
      cols=[];
      temp=aray(1); temp2=aray(3);
      for i=1:size(aray,2)  % ie. 1:12
           if((aray(i)==temp) & (aray(i+2)==temp2))
               cnt=cnt+1;
               cols=[cols i];
           end
      end

     if(cnt==3)
            tjx=aray(1); tjy=aray(3);
            aray([cols cols+2])=[];
            tjvs=[tjvs ; tjx tjy aray];
     else
            temp=aray(2);temp2=aray(4);
            cnt=0;
            cols=[];
            for i=1:size(aray,2)  % ie. 1:12
                 if((aray(i)==temp) & (aray(i+2)==temp2))
                  cnt=cnt+1;
                     cols=[cols i];
                 end
            end

                if(cnt==3)
                  tjx=aray(2); tjy=aray(4);
                  aray([cols cols+2])=[];
                  tjvs=[tjvs ; tjx tjy aray];
                end

      end

     clear aray;
     clear cols;
  end
%=========================================================================
% Here before proceeding, we can eliminate any bad triple junctions
% outside the dimension values by just checking the first column of
% tjvs for x limits and second column for y limits.
%=========================================================================
rows=[];
for i=1:noTriB
    if (tjvs(i,1) <0) | (tjvs(i,1)> X_length*GrainSz)
```

```
        rows=[rows i];
    end
    if (tjvs(i,2) <0) | (tjvs(i,2)> Y_width*GrainSz)
        rows=[rows i];
    end
end

tjvs(rows,:)=[];
clear rows;
% Now tjvs contain the actual triple junctions

%=========================================================================
% Process of converting vertices into rectangular coordinates and
% corresponding triple junction to origin
%=========================================================================

reccds=tjvs; % store triple junction coordinates

% Make each triple junction an origin by substracting triple junc x
from all boundary Xs and similarly y.
    reccds(:,3)=reccds(:,3)-reccds(:,1);
    reccds(:,5)=reccds(:,5)-reccds(:,1);
    reccds(:,7)=reccds(:,7)-reccds(:,1);
    reccds(:,4)=reccds(:,4)-reccds(:,2);
    reccds(:,6)=reccds(:,6)-reccds(:,2);
    reccds(:,8)=reccds(:,8)-reccds(:,2);
    % Makes the first two columns zeros it triple junctions as origins
    reccds(:,1)=reccds(:,1)-reccds(:,1);
    reccds(:,2)=reccds(:,2)-reccds(:,2);
    % Delete the first two columns as there is no more need of it
    reccds(:,1:2)=[];     % Now the final format of reccds is x1 y1 x2
y2 x3 y3


%=========================================================================
% code for finding grain boundary angles and arranging the vertices
% accordingly (taking advantage of quadrant)
%=========================================================================
% bdwang[]will contain the vertices of 3 boundaries of a triple
% junction with angle each boundary makes with X-axis or  direction of
% current flow. here each triple junc. is made as origin first for
% finding the quadrant of each boundary vertex and then the angle of
% each boundary.

bdwang =[];

for i= 1 : size(reccds,1)
vwa=[];
for j=1:3
quad(j,1)=0;
% quad will be a 3x3 matrix after this loop with first column as zeros
quad(j,2)=reccds(i,2*j-1);
% ans 2nd, 3rd columns as x and y co-ordiantes
quad(j,3)=reccds(i,2*j);
```

```
end

for k=1:3
quadang=quad(k,1);
a=quad(k,2);
b=quad(k,3);

if(a==0 & b~=0)
      if (b>0) quadang=90;
      else quadang=270;
      end
      elseif(b==0 & a~=0)
      if(a>0) quadang=0;
      else quadang=180;
      end
else

if( (a>0 & b>0) | (a<0 & b>0) ) quadang = atan2(b,a)*180/pi;
 % atan2 range is -pi to pi
elseif( (a<0 & b<0) | (a>0 & b<0) ) quadang = 360 + …atan2(b,a)*180/pi;
else fprintf(' here x=0 and y=0 that means a boundary is missing');
break;
end
end
quad(k,1)= quadang;
clear a b quadang;
end  % quad will still  be a 3x3 matrix after this loop with first
     % column containing angle of that coordinate/boundary
quadcol=quad(:,1);
quadcol=sort(quadcol);

for m=1:3
    temp=quadcol(m);
     for n=1:3
       if(quad(n,1)==temp)
         row=n;
         end
      end
vwa =[vwa quad(row,2) quad(row,3) quad(row,1)];
 % vwa contains x1,y1,angle1,x2,y2,angle2,x3,y3,angle3 and
 % ang1<ang2<ang3
end
 bdwang=[bdwang ; vwa];
 end


%=========================================================================
% Code for converting bdwang to actual boundary vertices with angles.
%=========================================================================
ActBdWAng=[];
radian=pi/180;
rand('state' ,5);
```

```
for i= 1 : size(reccds,1)
Theta1=rand*60; if(Theta1<=37) Theta1= sin((Theta1/2.0)*radian);
else Theta1= sin((37.0/2.0)*radian); end;
Theta2=rand*60; if(Theta2<=37) Theta2= sin((Theta2/2.0)*radian);
else Theta2= sin((37.0/2.0)*radian); end;
Theta3=rand*60; if(Theta3<=37) Theta3= sin((Theta3/2.0)*radian);
else Theta3= sin((37.0/2.0)*radian); end;

DeltaY= Theta1*cos(bdwang(i,3)*radian) + Theta2*cos(bdwang(i,6)*radian)
...+ Theta3*cos(bdwang(i,9)*radian);

ActBdWAng=[ActBdWAng; tjvs(i,1) tjvs(i,2) bdwang(i,1)+tjvs(i,1)...
...bdwang(i,2)+tjvs(i,2) bdwang(i,3) bdwang(i,4)+tjvs(i,1)
...bdwang(i,5)+tjvs(i,2) bdwang(i,6) bdwang(i,7)+tjvs(i,1)
...bdwang(i,8)+tjvs(i,2) bdwang(i,9) DeltaY];
end
=====================================================================
% Here the ActBdWAng: Actual Boundary Vertices With angles contain the
%  following format
%   [TripleJuncX   TripleJuncy   boundary1X   boundary1Y   boundary1Ang
%boundary2X boundary2Y boundary2Ang boundary3X boundary3Y boundary3Ang
%DeltaY] Where boundar1, 2, 3 are boundaries that makes angles in
%ascending  order measured from X-axis in counter clockwise direction.
% Insted of DeltaY, We can directly calculate the flux divergence in
%same loop and replace with DeltaY in ActBdWAng(12)
%=====================================================================

%============ELECTROMIGRATION DATA FOR MATERIAL USED (Al)==============

Omega=1.7e-23;    % in CC   Omega is inverse of N(concentration)
D0=1e-4;          % cm2/sec
K=1.3807e-23;     % J/K
Zstar=1.6;
Q0=9.61314e-20;   % in Jolue = 0.6eV, GB activation energy for Al
Rho0=2.65e-6 ;
Alpha=0.0039;     % per Degree Centigrade
q=1.602e-19;      % Couloumb of electron charge
ThermalCond = 2.37; %  Thermal Conductivity in Watt/cm K
MeltingPt= 933;  % in K ie.660C
delta = 10e-8 ;

%======================STRESS CONDITIONS==============================
T0=325;  TAvg=T0; T_Max=T0;
% K  initially Agerage Temp = Room Temperature or Initial Temp

Current=130e-3;           % Current in ampers
h=0.5e-4 ;                % thickness of beam in cm
w=Y_width*GrainSz*1e-4;   % Width of MEMS Beam
J=Current/(w*h) ;         % Current Density in amp/cm2
flag =1;
Time=0;
TimeInc=360000;           % seconds
dia=[];
```

```
L=X_length*GrainSz*1e-4;  %cm
Area= w*h;                % Sq.Cm

R=(Rho0*(1+Alpha*(T0-300)))*L/Area;

FluxDivConst=(D0*Zstar*q)/(Omega*K) ;
% Here J and T ARE not included as they vary with time and
% position. They are locally found out at every Triple junction

DiffCoeffExpConst=-Q0/K;
MaxCount=0;
MaxVoidDia=0;
MaxWidthLost=0;
ActBdWAng(:,13:14)=0;
% INITIALLY TOTAL MASS DIFFUSED(13th colum) IS ZERO hence diameter of
% voids is also zero (14th column)

Iteration=0;
No_of_Divisions =2000;
Temps(1:No_of_Divisions+1)=T0;  % Initially Temperature at every point
is ambient
BeamLength=0:L/No_of_Divisions:L;
ColLength= L/No_of_Divisions  ;
% Column length for descritising the strip in to elements. Make this
% small for accuracy.
NegFlxDivTj=[];
PlotData=[];
void=[];


%===================== THE BEGINNING OF MAIN EM PROGRAM===============

while flag==1

Iteration=Iteration+1;
for i=1:size(ActBdWAng,1)
set=[];
TmpWidth=w;
count=0;
=========================================================================
% USING LOCAL TEMPERATURE FOR LOCAL PROPERTIES CALCULATION
=========================================================================

for C=1:No_of_Divisions
  if(C*ColLength*1e4 >ActBdWAng(i,1))
    T= (Temps(C)+Temps(C+1))/2;
  end
end
Rho=Rho0*(1+Alpha*(T-300));
% Rho value in a particular Triple junction or for the CLOUMN in
% which it lies
%=========================================================================
% CODE FOR LOCAL CURRENT DENSITY AT THAT PARTICULAR TRIPLE JUNCTION
```

```
%=====================================================================
ActBdWAng(i,1)
       for C=1:No_of_Divisions
         if(C*ColLength*1e4 >ActBdWAng(i,1))
        Xmin= (C-1)*ColLength ; Xmax=(C)*ColLength;
         break;
% the current Triple junction lies in this column. And we have to find
% other triple junctions with negative flux divergences lying in same
% column to find actual current density at that junction
         end
       end

for j=1:size(NegFlxDivTj,1)  % This should not get executed in first
iteration as size is 1
if(NegFlxDivTj(j,1)>Xmin*1e4 & NegFlxDivTj(j,1)<Xmax*1e4)
% here multiplied by e4 as matlab Vornoi coords have no units
count=count+1;
set=[set;NegFlxDivTj(j,:)];
end
end


if( count>=1) % Means one or more voids in the column range considered
TmpWidth= w-sum(set(:,3));  % Reduction in Width due to Void of
Diameter=dia in set(count,3)
else
TmpWidth=w; % ie. no voids in current column so width is actual width w
end

J=Current/(TmpWidth*h);

% End of CODE FOR LOCAL CURRENT DENSITY AT a PARTICULAR TRIPLE JUNCTION
%=====================================================================
FluxDiv=(FluxDivConst*Rho*J/T) * exp(DiffCoeffExpConst/T);
TempDelJ=ActBdWAng(i,12)*FluxDiv;     % becomes Del.J
=====================================================================
% CLACULATION OF NO OF ATOMS ACCUMULATED OR DEPLETED AT CURRENT TRIPLE
% JUNCTION
=====================================================================
ActBdWAng(i,13)=ActBdWAng(i,13)+TempDelJ*delta*h*TimeInc;     % Since
DeltaN=delta*h*Del.J* Time
end

NegFlxDivTj=[];
for i=1:size(ActBdWAng,1)
if ActBdWAng(i,12)<0  % if DeltaY is -ve ie. negative flux divergence
if(ActBdWAng(i,13)>0) keyboard; end;
dia=  sqrt(-1*ActBdWAng(i,13)*Omega/(pi*h));  % in cm

if (dia >MaxVoidDia) MaxVoidDia=dia; end;
% to know the maximum void Diameter
NegFlxDivTj=[NegFlxDivTj; ActBdWAng(i,1) ActBdWAng(i,2) dia];
end
end
```

```
void= [void; Time NegFlxDivTj(floor(size(NegFlxDivTj,1)/2) ,3)
MaxVoidDia]

qDot=0;                % Heat generated per unit volume    Watt/cc
Tprev=T_Max;

Xmin=0-ColLength; Xmax=0;
Rset=[];
Tcount=0;
for Column=ColLength:ColLength:L
        Tcount=Tcount+1;
        count=0;
        set=[];
        TmpWidth=w;

        Xmin=Xmin+ColLength;
        Xmax=Xmax+ColLength;

        TColAvg=(Temps(Tcount) + Temps(Tcount+1))/2;
% Average Temperature of that Particular column.


for j=1:size(NegFlxDivTj,1)
if(NegFlxDivTj(j,1)>Xmin*1e4 & NegFlxDivTj(j,1)<Xmax*1e4)
% here multiplied by e4 as matlab Vornoi coords have no units
count=count+1;
set=[set;NegFlxDivTj(j,:)];
end
end

if count>=MaxCount
MaxCount=count;    % to know maximum number of voids in any column
VoidSet=set;
end;

if count>=1
if (sum(set(:,3))>MaxWidthLost) MaxWidthLost=sum(set(:,3));
% to know maximum width lost at any c/s
MaxwidthSet=set;
% this stores the column having voids whose sum  is maximum
end;
end;

if( count>=1)    % Means one or more voids in the column range
considered
TmpWidth=w-sum(set(:,3));
else
TmpWidth=w; % ie. no voids in current column so width is actual width w
end

if(TmpWidth <=0.5*w)
critical
break;  % Out of (for Column=ColLength:ColLength:L) loop
```

```
end

DeltaT=TColAvg-300;
Rho=Rho0*(1+Alpha*DeltaT);
TempR= Rho*ColLength/(TmpWidth*h);
qDot=qDot+((Current/(TmpWidth*h))^2) *Rho;  % heat generated= j^2 * rho
Rset=[Rset TempR];
end  % for Column=ColLength:ColLength:L

if(TmpWidth <=0.5*w)
fprintf(1,'\n c/s area is zero or less look above for final percentage
change in resistance')
break; % Out of while loop, following statements are not executed end

TotalR= sum(Rset);
% if no voids then TotalR should be equal to Original R. if there are
% voids this shud be greater than R
PrcntChng =(TotalR-R)*100/R
qDot=qDot/No_of_Divisions;
T_Max= T0+(qDot*L^2)/(8*ThermalCond)
TAvg=(T_Max+T0)/2

========================================================================
% CODE FOR TEMPERATURE PROFILE IN BEAM FOR NEXT TIME STEP CALCULATIONS
% ITS ASSUMED THAT THIS TEMPERATURE PROFILE WILL EXIST FROM CURRENT
% TIME TO NEXT INCREMENTAL TIME
========================================================================

for c=0: No_of_Divisions
x=c*ColLength;
Temps(c+1)=T0+qDot*(L*x-x^2)/(2*ThermalCond);
end


plot(BeamLength,Temps,'-');
xlabel('Beam length (cm)');
ylabel('Temperature (K)')
title('Temperature Profile in the Beam during EM Failure');
hold on;

% ================CHECKING THE FAILURE CRITIRIA====================

if (PrcntChng>=15)
fprintf(1,' Failure of first kind ie. Resistance increased beyond
allowable limit 40% \n\n');

flag=0;    % Exit the While Loop
fprintf(1,' Time To Failure = %f Seconds i.e. %f Hours or %f Years \n
\n', Time, Time/3600.0, Time/(60*60*24*365));
RunTime=cputime-StartTime;
fprintf(1,'Total Run time for this simulation=%f Minutes \n \n',
RunTime/60.0);
fprintf(1,'Maximum number of voids in any column = %f with Diameters
```

```
fprintf(1,'\n Maximum Void Dia =%f \n  Maximum WidthLost=
%f\n',MaxVoidDia,MaxWidthLost);
break;

elseif (T_Max>=0.5*MeltingPt)
fprintf(1,' Failure of Second kind ie. Tempeaure is greater than Half
...the Melting Pt ...Possible Creep failure \n\n');
flag=0;    % Exit the While Loop
fprintf(1,' Time To Failure = %f Seconds i.e. %f Hours or %f Years \n
...\n', Time, Time/3600.0, Time/(60*60*24*365));
RunTime=cputime-StartTime;
fprintf(1,'Total Run time for this simulation=%f Minutes \n \n',
RunTime/60.0);
fprintf(1,'Maximum number of voids in any column = %f with Diameters
...',MaxCount); fprintf(1,' %e\n',VoidSet);
fprintf(1,'\n Maximum Void Dia =%f \n  Maximum WidthLost=
...%f\n',MaxVoidDia,MaxWidthLost);
break;

elseif (T_Max-Tprev <0.0001)    % Diff betwen prevoius and current
temperatures is lessthan 0.01%
fprintf(1,' Temperature Difference converged to %f which is below 0.011
Percent.\n \n',T_Max-Tprev);
flag=0;    % Exit the While Loop
fprintf(1,' Time for Convergence = %f Seconds i.e. %f Hours or %f Years
...\n \n', Time, Time/3600.0, Time/(60*60*24*365));
RunTime=cputime-StartTime;
fprintf(1,'Total Run time for this simulation=%f Minutes \n \n',
...RunTime/60.0);
fprintf(1,'Maximum number of voids in any column = %f with Diameters
...',MaxCount); fprintf(1,' %e',VoidSet);
fprintf(1,'\n Maximum Void Dia =%f \n  Maximum WidthLost=
...%f\n',MaxVoidDia,MaxWidthLost);

else
Time=Time+TimeInc

end


PlotData=[PlotData ; Time/3600 TotalR PrcntChng T_Max TAvg];


end   % end while

%============================END OF MAIN PROGRAM=======================

%=========================PLOT TOTAL RESISTAVNE VS TIME=============
figure(3)
plot(PlotData(:,1),PlotData(:,2));
title('Total Resistance Vs Time');
ylabel('Total Resistance(Ohms)');
xlabel(' Time (hrs)');
```

```
%============PLOT TOTAL % INCREASE IN RESISTAVNE VS TIME=============
figure(4)
plot(PlotData(:,1),PlotData(:,3));
%Percent change in Resistance  Vs Time on X axis
title(' Percent change in Resistance Vs Time');
ylabel('Percentage change in Resistance');
xlabel(' Time (hrs)');

%==========PLOT % RESISTANCE CHANGE VS MAX BEAM TEMPERATURE==========
figure(5)
plot(PlotData(:,4),PlotData(:,3));
% Percent change in Resistance Vs  TMax
title(' Percent change in Resistance Vs Maximum Beam Temperature');
ylabel('Percentage change in Resistance');
xlabel(' Maximum Beam Temperature (K)');

%======================SAVE WORK SPACE==============================
fid = fopen('PlotData.txt','w');
fprintf(fid,' %10.4f %10.4f %10.4f %10.4f %10.4f \n',PlotData');
fclose(fid);
xlswrite('WithJHandEM.xls',PlotData,'Sheet1','A');
save('PlotData.mat','PlotData','NegFlxDivTj');

%================PLOT THE FINAL EM DEGRADED STRIP VISUAL ========
figure(6)
line(0:200, zeros(1,201));
line(0:200, ones(1,201)*20);
line(zeros(1,21), 0:20);
line(ones(1,21)*200, 0:20);
hold on
for i=1:size(MaxwidthSet,1)
circle(MaxwidthSet(i,1),MaxwidthSet(i,2),MaxwidthSet(i,3)*1e4);
hold on;
end

%=========================PLOT VOID GROWTH HISTORY================
figure(7)
plot(void(:,1), void(:,2)*1e4)
title(' void Size in mu vs time');
ylabel('void size in microns');
xlabel(' time (K)');
```